

# Constraining models of postglacial rebound using space geodesy: a detailed assessment of model ICE-5G (VM2) and its relatives

Donald F. Argus<sup>1</sup> and W. Richard Peltier<sup>2</sup>

<sup>1</sup>*Jet Propulsion Laboratory, California Institute of Technology, Pasadena, CA, 91109, USA. E-mail: donald.f.argus@jpl.nasa.gov*

<sup>2</sup>*Department of Physics, University of Toronto, Toronto, ON, M5S 1A7, Canada*

Accepted 2010 February 11. Received 2010 February 10; in original form 2009 August 27

## SUMMARY

Using global positioning system, very long baseline interferometry, satellite laser ranging and Doppler Orbitography and Radiopositioning Integrated by Satellite observations, including the Canadian Base Network and Fennoscandian BIFROST array, we constrain, in models of postglacial rebound, the thickness of the ice sheets as a function of position and time and the viscosity of the mantle as a function of depth. We test model ICE-5G VM2 T90 Rot, which well fits many hundred Holocene relative sea level histories in North America, Europe and worldwide. ICE-5G is the deglaciation history having more ice in western Canada than ICE-4G; VM2 is the mantle viscosity profile having a mean upper mantle viscosity of  $0.5 \times 10^{21}$  Pa s and a mean uppermost-lower mantle viscosity of  $1.6 \times 10^{21}$  Pa s; T90 is an elastic lithosphere thickness of 90 km; and Rot designates that the model includes (rotational feedback) Earth's response to the wander of the North Pole of Earth's spin axis towards Canada at a speed of  $\approx 1^\circ \text{ Myr}^{-1}$ .

The vertical observations in North America show that, relative to ICE-5G, the Laurentide ice sheet at last glacial maximum (LGM) at  $\approx 26$  ka was (1) much thinner in southern Manitoba, (2) thinner near Yellowknife (Northwest Territories), (3) thicker in eastern and southern Quebec and (4) thicker along the northern British Columbia–Alberta border, or that ice was unloaded from these areas later (thicker) or earlier (thinner) than in ICE-5G. The data indicate that the western Laurentide ice sheet was intermediate in mass between ICE-5G and ICE-4G. The vertical observations and GRACE gravity data together suggest that the western Laurentide ice sheet was nearly as massive as that in ICE-5G but distributed more broadly across northwestern Canada.

VM2 poorly fits the horizontal observations in North America, predicting places along the margins of the Laurentide ice sheet to be moving laterally away from the ice centre at  $2 \text{ mm yr}^{-1}$  in ICE-4G and  $3 \text{ mm yr}^{-1}$  in ICE-5G, in disagreement with the observation that the interior of the North American Plate is deforming more slowly than  $1 \text{ mm yr}^{-1}$ . Substituting VM5a T60 for VM2 T90, that is, introducing into the lithosphere at its base a layer with a high viscosity of  $10 \times 10^{21}$  Pa s, greatly improves the fit of the horizontal observations in North America. ICE-4G VM5a T60 Rot predicts most of the North American Plate to be moving horizontally more slowly than  $\approx 1 \text{ mm yr}^{-1}$ , in agreement with the data.

ICE-5G VM5a T60 Rot well fits both the vertical and horizontal observations in Europe.

The space geodetic data cannot distinguish between models with and without rotational feedback, in the vertical because the velocity of Earth's centre is uncertain, and in the horizontal because the areas of the plate interiors having geodetic sites is not large enough to detect the small differences in the predictions of rotational feedback going across the plate interiors.

**Key words:** Satellite geodesy; Global change from geodesy; Glaciology; Dynamics: gravity and tectonics; Kinematics of crustal and mantle deformation.

## 1 INTRODUCTION

Elevated beach terraces along the coastlines of Canada and Scandinavia record Earth's isostatic response to unloading of the ice sheets

since the last glacial maximum (LGM) at  $\approx 26$  ka (26 000 yr BP), and coral reefs in the tropics record the resulting rise of global sea level. Relative sea level histories determined by radiocarbon dating of beach terraces (e.g. Peltier 2002a) and Uranium–Thorium dating

of coral reef deposits are the main observations constraining viscoelastic models of postglacial rebound (Peltier 1994, 1996, 2004; Kaufmann & Lambeck 1997; Milne *et al.* 2001; Peltier & Fairbanks 2006; Paulson *et al.* 2007; Sella *et al.* 2007). Such models account for both the transformation of the ice sheets into ocean water and the gravitational response of the oceans to the resulting deformation of solid Earth. The models depend on three correlated parameters: the mass of the ice sheets as a function of position and time, the viscosity of the mantle as a function of depth, and the thickness of the elastic lithosphere.

Space geodesy is now providing an exciting means by which to further constrain such postglacial rebound models. First, estimates of vertical site motion well constrain former ice sheet thickness in the interiors of the continents (insofar as the timing of the unloading of the ice sheets is well constrained by glacial geomorphology), where the ice sheet thickness is unconstrained by relative sea level histories. Second, estimates of horizontal site motion newly constrain the rheology of the lithosphere and mantle.

In this study, we evaluate postglacial rebound models with observations from global positioning system (GPS), satellite laser ranging (SLR), very long baseline interferometry (VLBI) and Doppler Orbitography and Radiopositioning Integrated by Satellite (DORIS), including data from the (CBN) Canadian Base Network (M. Craymer, National Resources Canada, electronic communication, 2006) and the Fennoscandian BIFROST network (Johansson *et al.* 2002). At the heart of the analysis in this study is distinguishing between postglacial rebound, plate motion and (rotational feedback) Earth's response to the wander of the North Pole of Earth's spin axis towards Canada at  $\approx 1^\circ \text{ Myr}^{-1}$ . An important element distinguishing this study from others is that we also estimate the velocity of Earth's centre, the reference relative to which vertical motions are described, rather than assuming the velocity of Earth's centre to be that estimated using SLR observations of NASA's LAsER GEODYnamics Satellite (LAGEOS).

## 2 MODELS OF POSTGLACIAL REBOUND AND ROTATIONAL FEEDBACK

We compare the space geodetic observations against elements of the models of Peltier (1994, 1996, 2004, 2007) and Peltier & Drummond (2008), but focus on the last two models. The main basis on which the models are constructed is a global data base of many hundred relative sea level (RSL) histories (Peltier 2007, fig. 16). We know of no other global models of postglacial rebound that are generally available to the international community. Peltier & Luthcke (2009) present a detailed analysis of Earth's rotational response to glacial isostatic adjustment, emphasizing the high quality fit of the theory to both the non-tidal acceleration in the rate of rotation and the speed and direction of the wander of the spin axis.

In this study, we evaluate the impact on the fit to the space geodetic observations of varying four elements of the postglacial rebound models: the ice sheet thickness as a function of position and time, the viscosity of the mantle as a function of depth, the thickness of the elastic lithosphere, and whether or not we include the effect of rotational feedback, which is dominated by Earth's response to the wander of the North Pole of the spin axis towards Canada at  $\approx 1^\circ \text{ Myr}^{-1}$  over the past 100 yr as observed by the International Latitude Service. Earth also deforms in response to the non-tidal acceleration in Earth's rate of rotation (Stephenson & Morrison 1995), but this deformation is negligible relative to that generated by polar wander.

### 2.1 Ice sheet models

We compare the space geodetic observations against two models of ice sheet thickness as a function of time, ICE-4G (Peltier 1994, 1996, 2002b) and ICE-5G (Peltier 2004, 2007; Peltier & Drummond 2008; Fig. 1). In this study, we compare against the version of ICE-4G in Peltier (2002b) and ICE-5G version 1.3a (Peltier 2007).

In North America the Laurentide ice sheet at LGM is about 25 per cent more massive in ICE-5G than in ICE-4G (Fig. 1). East of Hudson Bay ice sheet thickness in the two models is nearly the same. West of Hudson Bay there is in ICE-5G at LGM a 4000 m thick Keewatin ice dome, much thicker than the 2500 m thick ice sheet there in ICE-4G. Furthermore in ICE-5G at LGM a 4000 m thick ice ridge extends from the Keewatin dome south through Lake Winnipeg [southern Manitoba], whereas in ICE-4G there is no such ridge and the ice is only 2500 m thick.

Peltier (2002a, 2004) greatly increased the thickness of the western Laurentide ice sheet in ICE-4G to that in ICE-5G in order to fit early VLBI and GPS estimates of uplift at Yellowknife (Argus *et al.* 1999), to fit early estimates of the time rate of change of gravity at Earth's surface observed using absolute gravimeters along a profile from Churchill (on Hudson Bay) through Manitoba and Minnesota into Iowa (Lambert *et al.* 2001), and to increase total sea level rise since LGM by  $\approx 12 \text{ m}$  to 120 m to fit relative sea level observations at coral reefs from the island of Barbados in the Caribbean Sea (Peltier & Fairbanks 2006, fig. 5). However, the GPS and VLBI results that we present herein, which are based on a significantly longer time-series than those in Argus *et al.* (1999), suggest that the western Laurentide ice sheet was less massive than that in ICE-5G.

In Europe the Fennoscandian ice sheet at LGM in ICE-5G is nearly identical to that in ICE-4G. The ice sheet in the Barents Sea is also similar in the two models. The ice sheet in Novaya Zemlya, the Kara Sea, and northern continental Russia at LGM is either thinner in ICE-5G than in ICE-4G or absent in ICE-5G, satisfying the results of the (QUEEN) Quaternary Environment of the Eurasian North project (Svendsen *et al.* 2004; Peltier 2004).

The Antarctica and Patagonian ice sheets in ICE-5G at LGM are identical to those in ICE-4G. In ICE-5G (version v1.3a) roughly half of the excess Antarctic ice sheet at  $\approx 26 \text{ ka}$  disintegrates quickly during meltwater pulse 1b at 11 ka, as inferred on the basis of the RSL data at Barbados (Peltier & Fairbanks 2006) and radiocarbon dating of the onset of marine sedimentation at many sites on the Antarctic shelf that constrain the retreat of the ice from the shelf break to be at  $\approx 11 \text{ ka}$  (Leventer *et al.* 2006). In ICE-4G the excess ice disintegrates more gradually between 11 and 4 ka (Fig. 1).

### 2.2 Mantle viscosity models

We compare the space geodetic observations against three models of mantle viscosity as a function of depth, VM1 (Peltier 1994), VM2 (Peltier 1996, 2004) and VM5a (Peltier & Drummond 2008; Fig. 2). In all the models viscosity is laterally invariant. While the upper mantle above subducting slabs [e.g. Vancouver Island (James *et al.* 2009)] and hotspots [e.g. Iceland (Pagli *et al.* 2007)] may be significantly less viscous than elsewhere, we maintain that throughout most of the mantle temperature and pressure increase along an adiabat (Turcotte & Schubert 1982), and therefore the mantle viscosity in areas near neither subduction zones, mid-ocean ridges, nor hotspots is laterally nearly invariant. Because the Rayleigh number of the mantle is high, heat transfer is mainly by convection and not conduction, and the horizontal distance over which mantle viscosity

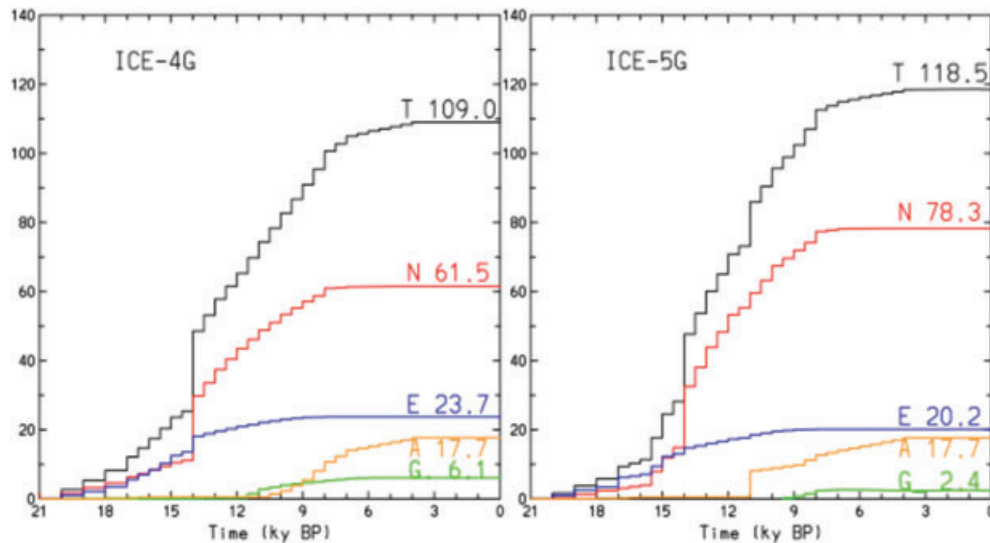


**Figure 1.** Mean sea level as a function of time for ICE-4G and ICE-5G (v1.3a) broken down into the ice sheet causing sea level rise (T, Total; N, North America; E, Eurasia; A, Antarctica; G, Greenland). The mean sea level values are computed using the method of Peltier (2005) and Peltier & Fairbanks (2006), which does not use the ‘implicit ice’ method.

varies beneath spreading centres and subduction zones is believed to be small, on the order of the thickness of the thermal surface boundary layer (the lithosphere), as in the convection models of Solheim & Peltier (1994). In any case we wish to test the hypothesis that a mantle that is laterally invariant can fit all the observations.

VM1 is a two layer model in which the upper mantle and transition zone have a viscosity of  $1 \times 10^{21}$  Pa s, and the lower mantle has a viscosity of twice that. The boundary between the transition zone and lower mantle is at 660 km depth, the seismically observed depth at which the phase transformation from spinel to a mixture of perovskite and magnesiowustite occurs.

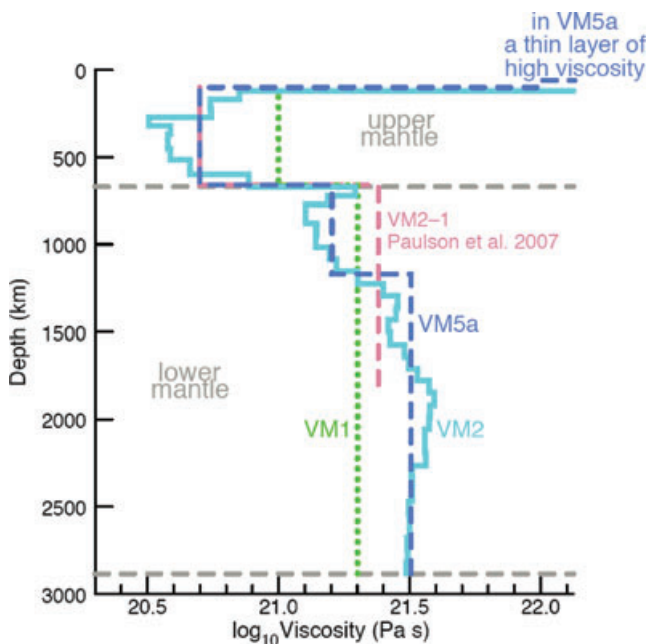


**Figure 2.** Mantle viscosity as a function of depth in VM1 (Peltier 1994), VM2 (Peltier 2006), VM5a (Peltier & Drummond 2008) and VM2-1 (Paulson *et al.* 2007). In VM5a a thin layer of high viscosity ( $10 \times 10^{21}$  Pa s) is between 60 and 100 km depth.

In VM2 the viscosity of the mantle varies in a detailed fashion as estimated by a formal Bayesian inversion of a subset of the RSL data that depend only weakly on the deglaciation history. Frechet kernels (Peltier 2004, fig. 5) show the range of mantle depths over which different observations constrain the viscosity. RSL histories from sites in Fennoscandia constrain the mean viscosity of the upper mantle and transition zone to be  $\approx 0.5 \times 10^{21}$  Pa s, about half that in VM1. In particular, VM2 fits the McConnell spectrum describing the relaxation time of Fennoscandian rebound as a function of horizontal wave number, whereas VM1 does not (Peltier 2004, fig. 4). Given the upper mantle viscosity in VM2, RSL histories from sites in Laurentia constrain the mean viscosity of the upper 500 km of the lower mantle to be  $\approx 1.6 \times 10^{21}$  Pa s. Two geophysical observables, the wander of Earth’s spin axis since 1900 (Gross & Vondrak 1999; Argus & Gross 2004) and the non-tidal acceleration of Earth’s rotation rate (Stephenson & Morrison 1995), constrain the viscosity of the remainder of the mantle to be  $\approx 3.2 \times 10^{21}$  Pa s (Peltier 2007, fig. 18).

VM5a differs from VM2 in two regards. First, VM5a is, beneath the lithosphere, a three layer approximation of VM2. Second, whereas in VM2 the lithosphere is entirely elastic and 120 km thick (Peltier 1996) or 90 km thick (Peltier 2004), in VM5a the lithosphere consists of an elastic layer 60 km thick above a highly viscous ( $10 \times 10^{21}$  Pa s) layer 40 km thick.

Paulson *et al.* (2007) find that, given the ice sheet thickness in ICE-5G plus or minus 20 per cent, VM2 is indeed consistent with RSL histories and GRACE gravity data in North America. Paulson *et al.*’s (2007) study is an independent validation of Peltier’s (2004, 2007, 2009) models, and rules out the hypothesis that the viscosity of the mantle increases by very much more across the 660 km depth horizon than the factor of 3–4 in either VM2 or VM5a.

### 2.3 Elastic lithosphere thickness

We compare the space geodetic observations against two values of the thickness of the elastic lithosphere, 90 km (Peltier 2007) and 60 km (Peltier & Drummond 2008). Decreasing the thickness of the elastic lithosphere increases the gradient in vertical motion along the margins of the former ice sheets (Peltier 1986).

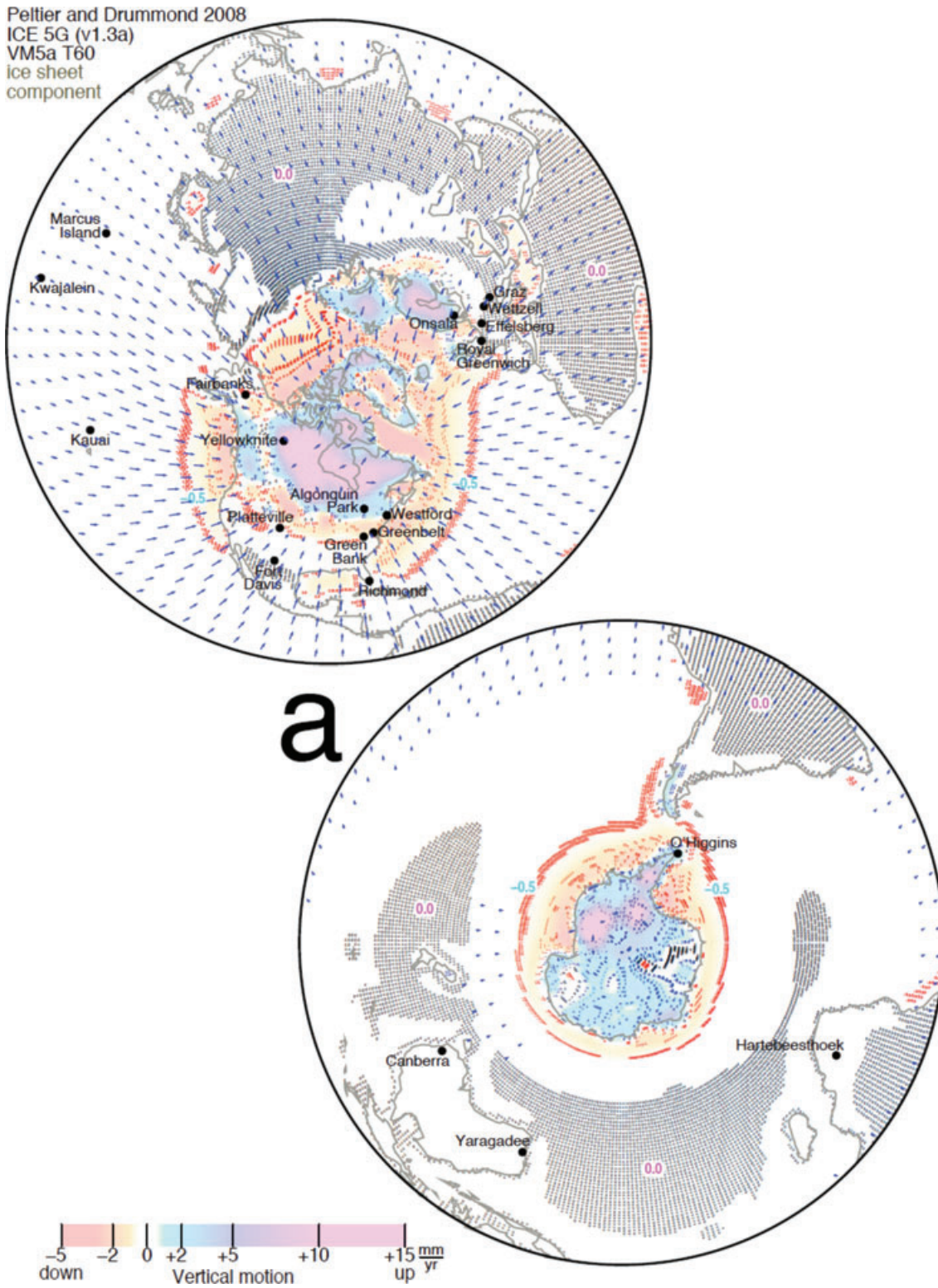


**Figure 3.** Predictions of the ICE-5G VM5a T60 Rot (Peltier & Drummond 2008) model: (a) the ice sheet component, (b) the rotational feedback component, and (c) the total. The colour gradations show the vertical predictions as the legend specifies. The tiny red and blue marks form contours at half  $\text{mm yr}^{-1}$  isospeeds of subsidence and uplift up to  $2 \text{ mm yr}^{-1}$ ; tiny black marks form grey areas where the vertical motion is  $0.0 \text{ mm yr}^{-1}$ . The blue arrows show the horizontal predictions and are omitted where less than  $0.5 \text{ mm yr}^{-1}$ . This equal area map does not preserve speed (the length of the arrow); the rotational feedback horizontal prediction is greatest at the poles and at the equator (at  $75^\circ \text{W}$  and  $105^\circ \text{E}$ ), where the predicted horizontal speed is  $1.5 \text{ mm yr}^{-1}$ .

2.4 Effect of rotational feedback

The models of Peltier (2004), Peltier (2007) and Peltier & Drummond (2008) consist of two components, an ice sheet component and a rotational feedback component (Fig. 3). The ice sheet component consists of solid Earth's viscoelastic response to unloading of the late Pleistocene ice sheets and the resulting loading of the ocean basins by water (ice and water surface loads). The ro-

tational feedback component consists of solid Earth's viscoelastic response to secular polar wander in the postglacial rebound model (centrifugal body force), which ultimately also results from ice sheet loss. The predictions of these models of the present-day wander of the North Pole of Earth's spin axis do not differ greatly (Peltier 2007, Tables 1 and 2) from the observed mean velocity of  $0.0035 \text{ arcsec yr}^{-1}$  along the  $79^\circ\text{W}$  meridian (Gross & Vondrak 1999; Argus & Gross 2004; see Appendix A). The models of Peltier (1994,

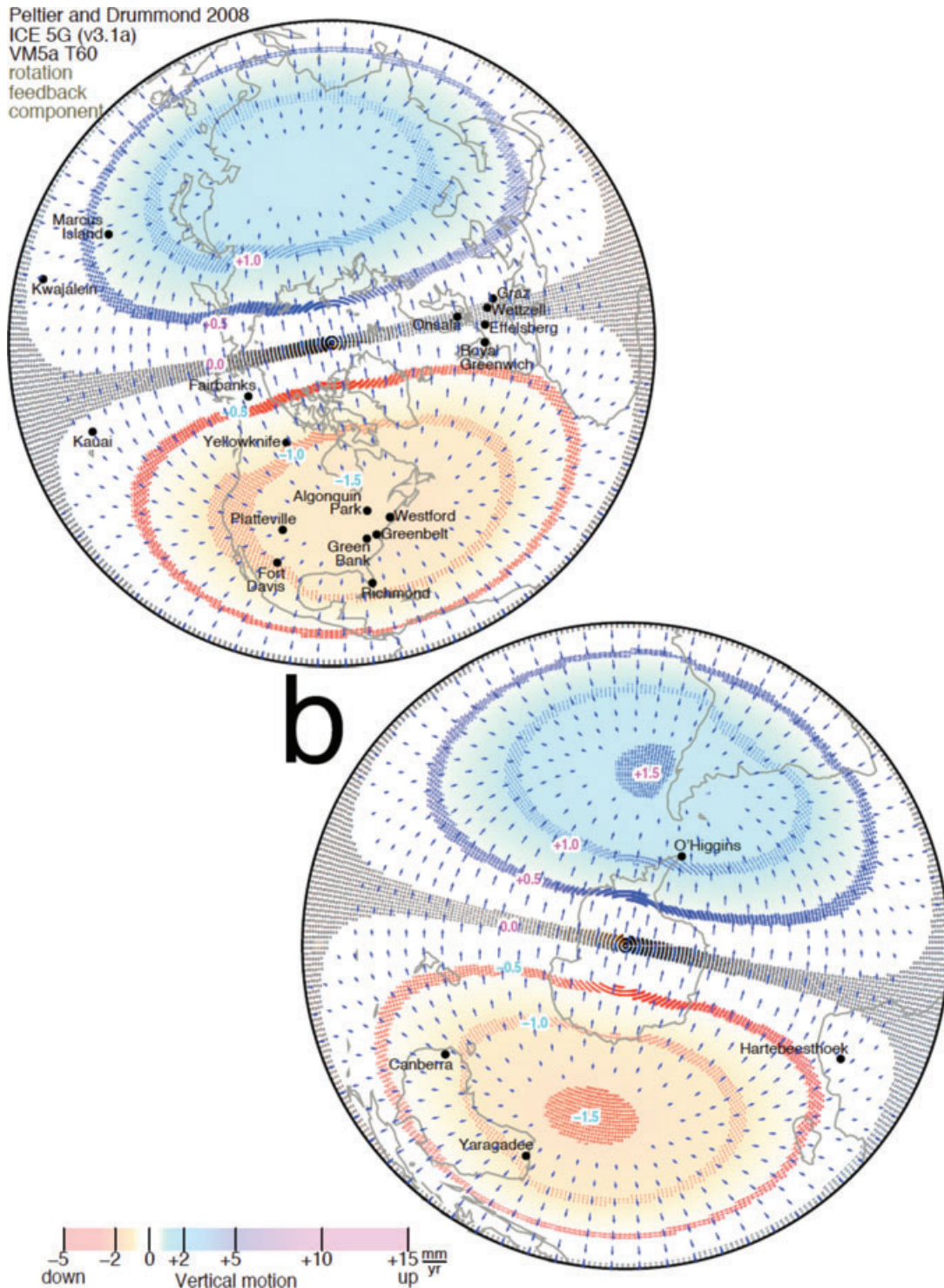


Figure 3. (Continued.)

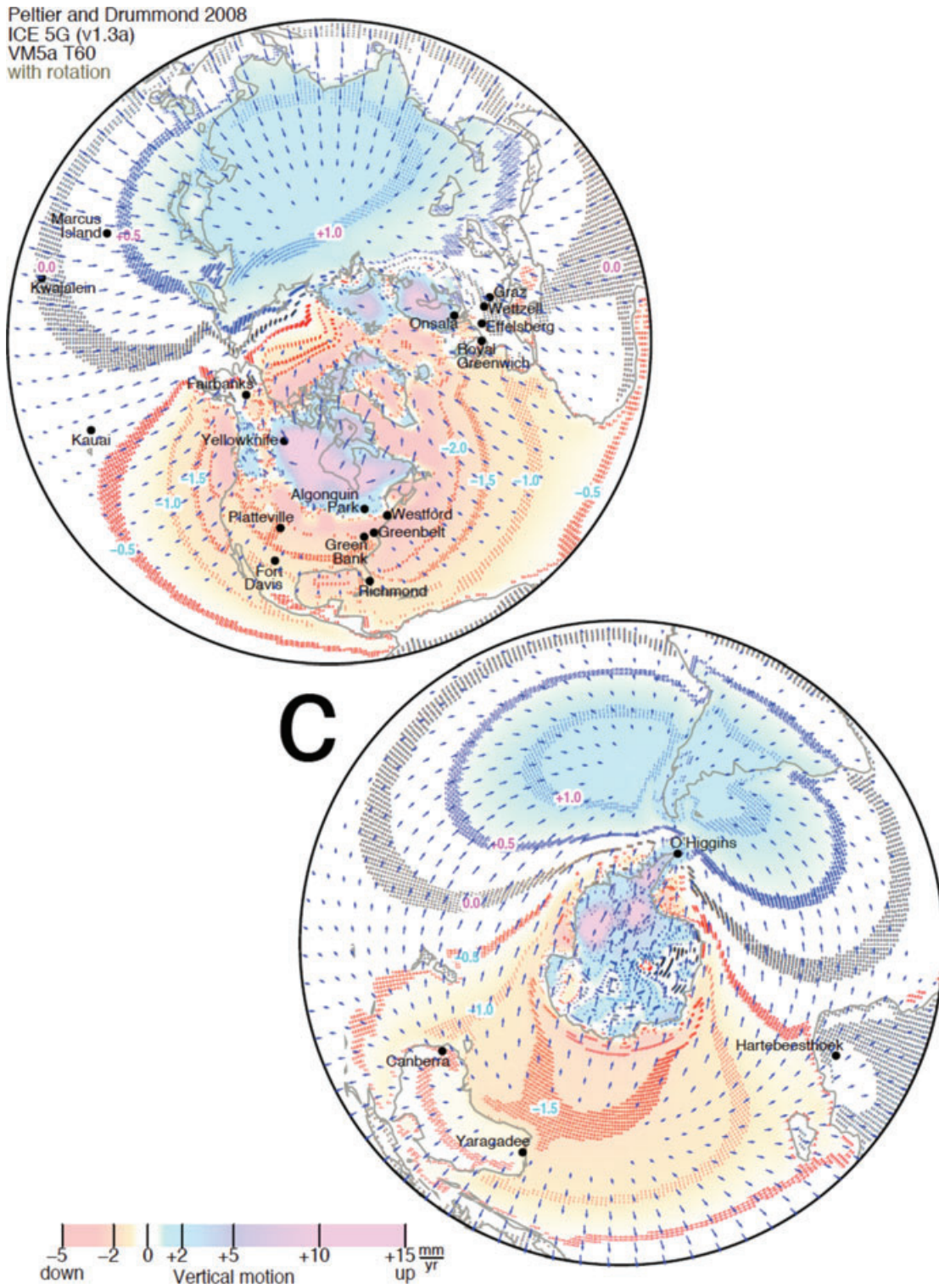


Figure 3. (Continued.)

1996) neglect the effect of rotational feedback. Herein we designate whether or not a postglacial rebound model includes rotational feedback using ‘Rot’ or ‘No Rot’. Rotational feedback generates, in the vertical, a degree-2 order-1 pattern with maximum uplift and subsidence of  $1.5 \text{ mm yr}^{-1}$  (in ICE-5G VM5a T60 Rot) at four locations along the  $75^\circ\text{W}$ – $105^\circ\text{E}$  great circle, two at  $45^\circ\text{N}$  and two at  $45^\circ\text{S}$ .

Rotational feedback also causes places to be moving horizontally away from the areas of subsidence and towards the areas of uplift. This sense is opposite that for postglacial rebound because Earth’s response to a body force (rotational feedback) differs from that to a surface force (postglacial rebound). Horizontal speed is a maximum of  $1.5 \text{ mm yr}^{-1}$  (in ICE-5G VM5a T60) at four locations along the

**Table 1.** Space geodetic site velocity solutions.

Technique	<i>N</i>	Time (yr)	Horizontal		Vertical		Time Period	Scientist [Institution]
			Dist (mm)	Sigma (mm yr <sup>-1</sup> )	Dist (mm)	Sigma (mm yr <sup>-1</sup> )		
GPS	319	6 (14)	4.5	0.7 (0.3)	10	1.6 (0.7)	1991–2007	Michael B. Heflin [Jet Propulsion Laboratory]
VLBI	32	11 (17)	6	0.7 (0.4)	13	1.3 (0.8)	1979–2000	Chopo Ma [Goddard Space Flight Center]
SLR	20	14 (18)	11	1.0 (0.7)	23	1.8 (1.3)	1976–2000	Richard J. Eanes [Center for Space Research]
DORI	38	10 (13)	19	1.9 (1.5)	31	3.1 (2.4)	1993–2006	Pascal Willis [Institut Geographique National]
BIF	53	8 (8)	4.5	0.9 (0.6)	10	1.5 (1.3)	1996–2004	Lidberg <i>et al.</i> 2007 [Onsala Space Observatory]
CBN	157	10 (11)	4.5	0.7 (0.6)	10	2.6 (2.0)	1994–2006	Michael Craymer [National Resources Canada]

*Notes:* *N*, number of sites; Time, median effective time period of observation; Dist, distance used to compute the systematic error in site velocity (as described in the text); Sigma, median standard error in velocity component. Values in parentheses are for the space technique's 10 tightest constrained site velocities. The velocity sigmas that we infer are comparable to those Williams *et al.* (2004) estimate using maximum likelihood estimation. Williams *et al.* (2004) estimate that, in two global sets of position time-series, flicker noise to be 5–11 mm in the horizontal and 20 to 23 mm yr<sup>-1</sup> in the vertical. Assuming flicker noise to be the main error source, and using eq. (32) of Bos *et al.* (2008), we find these to suggest systematic distance in the horizontal of 2–4 mm, and in the vertical of 7–8 mm, a little smaller than the 4.5 and 10 mm that we find. We and Williams *et al.* (2004) agree that the velocity sigmas are roughly 5–25 times greater than that inferred from linear propagation of position estimates.

75°W–105°E meridian, two along the equator and two at the North and South Poles.

In ICE-4G VM5a T60 Rot rotational feedback creates a nearly identical pattern but speeds are about one-third smaller (because the total ice mass in ICE-4G is less than that in ICE-5G), with maximum uplift and subsidence of 1.1 mm yr<sup>-1</sup> and maximum horizontal speed of 1.0 mm yr<sup>-1</sup>. In ICE-5G VM2 T90 Rot maximum uplift and subsidence are 1.8 mm yr<sup>-1</sup> and maximum horizontal speed is 1.2 mm yr<sup>-1</sup>.

RSL histories near the areas in which the degree-2 order-1 pattern of uplift and subsidence is greatest show the effect of rotational feedback to be close to that predicted by ICE-5G VM2 T90 Rot: east Patagonia and southern Japan (Ryukyu islands) rose up to ≈12 m over the past 8 kyr (a rate of 1.5 mm yr<sup>-1</sup>), and southern Australia subsided up to ≈6 m since 8 ka (a rate of 0.8 mm yr<sup>-1</sup>) (Peltier 2007, figs 21–25). Because these RSL data require the effect of rotational feedback to be large, we focus herein on comparisons of the space geodetic observations with models that include the effect of rotational feedback.

Mitrovica *et al.* (2005) find Earth's vertical response to rotational feedback to have maximum uplift and subsidence of just ≈0.25 mm yr<sup>-1</sup>, about six times less than predicted by the models of Peltier. However, Peltier & Luthcke (2009) show the formulation and prediction of Mitrovica *et al.* (2005) to be incorrect.

### 3 DATA

We invert six site velocity solutions from six institutions (Table 1). Four of the solutions are global. Twenty-one years of VLBI observations and 24 yr of SLR observation [more than the 13 yr of SLR observation in ITRF2005; Altamimi *et al.* 2007] tightly constrain velocities in places, contributing towards determining Earth's reference frame. Sixteen years of global GPS observations provide a superior geographic distribution to that of VLBI and SLR. Thirteen years of global DORIS observations provide estimates of site velocity that are not as tightly constrained as for the other three techniques. We completely describe this set of four global velocity solutions in Argus *et al.* (2010, appendix B).

Two of the velocity solutions are regional. Campaign GPS observations of the Canadian Base Network (CBN), with roughly 3–5 observations per site, and with 7–11 yr of data, are in the area beneath the former Laurentide ice sheet. Permanent GPS observations

of the BIFROST network provide information constraining Earth's response to the former Fennoscandian ice sheet.

The GPS velocity solution that we invert in this study differs from that in GEODVEL (Argus *et al.* 2010) in that we add 150 GPS sites on the interior of the North American Plate in the Continually Operating Reference Stations (CORS) and Forecast Systems Laboratory (FSL) networks. In this study, we determine model GEODVEL1b using means identical to that in GEODVEL except that we also invert these additional data.

## 4 METHODS

In this study we follow the methods of Argus *et al.* (1999, 2010) and Argus (2007).

### 4.1 Sites, places, plate interiors and glacial isostatic adjustment

#### 4.1.1 Sites

In general we define a site to correspond to a velocity provided to us by an analysis institution. A VLBI site consists of 1–3 radio telescopes less than 1000 m apart, an SLR site consists of 1–7 laser ranging stations less than 1000 m apart, and a DORIS site consists of 1–3 beacons less than 1000 m apart. [see Argus *et al.* (2010, appendix B) for three places at which we assume sites more than 1000 m apart to comprise a place.]

We define a GPS site more narrowly than for VLBI and SLR because we wish to carefully evaluate GPS estimates of site velocity, which are subject to uncertainty due to antenna substitutions. We define a GPS site to be an Antenna Reference Point (ARP); each GPS site has a unique four-letter abbreviation in the International GNSS Service (IGS). Thus we take GPS ARP's meters or tens of meters apart to be distinct sites. (This differs from the definition of a DOMES number, which groups ARP's near each other into a site.) In general we estimate an offset for a logged antenna substitution if the offset appears to be more than ≈10 mm in the vertical or more than ≈5 mm in the horizontal. If there is no logged antenna offset, we estimate a logged antenna substitution if the offset appears to be more than ≈12 mm in the vertical or more than ≈6 mm in the horizontal.

**Table 2.** Number of sites and places in (a) category rigid, (b) category glacial isostatic adjustment and (c) category omit.

VLBI	SLR	GPS	DORIS	CBN	BIFR	Plate	Sites	Places
(a) Category rigid								
1		7	5			Antarctica	13	10
		3				Arabia	3	3
3	2	15	4			Australia	24	13
5	9	56	2		9	Eurasia	81	47
		4	1			India	5	4
	1	4	2			Nazca	7	3
11	4	145	3	6		N. America	169	146
	1	6	5			Nubia	12	9
5	2	9	6			Pacific	22	15
1		7	3			S. America	11	6
		3	2			Somalia	5	3
26	19	259	33	6	9	Total	352	259
(b) Category glacial isostatic adjustment								
1		3	1			Antarctica	5	2
1		9	1		44	Eurasia	55	43
2		23	2	151		N. America	178	155
1	1	1				Macdonald	3	1
5	1	36	4	151	44	Total	241	201
(c) Category omit								
		1				Australia	1	1
1		3	1			Eurasia	5	2
		19				N. America	19	19
		1				Nubia	1	1
1		24	1			Total	26	23

*Notes:* A place in Category rigid is defined to consist of between 1 and 8 sites less than 30 km apart. A site or place in Category Rigid is on a plate interior, is not beneath or along the margin of a late Pleistocene ice sheet, and is used to estimate the angular velocity of a plate in GEODVEL1b. A site or place in Category Glacial Isostatic Adjustment is on a plate interior, has significant glacial isostatic adjustment (either uplift faster than  $2.5 \text{ mm yr}^{-1}$  or horizontal motions faster than  $0.5 \text{ mm yr}^{-1}$ ), and is not used to estimate the angular velocity of a plate in GEODVEL1b. We use the postglacial rebound model of Peltier [1996, ICE4G VM2 T90 No Rot] to evaluate whether a place is rising faster than  $2 \text{ mm yr}^{-1}$ . We use the model of Peltier [1994, ICE4G VM1 T60 No Rot] to evaluate whether a place is moving horizontally faster than  $0.5 \text{ mm yr}^{-1}$ . We use the models of Peltier (1996) and Peltier (1994) because they were the models that best fit, respectively, the horizontal and vertical geodetic observations when we determined GEODVEL [Argus *et al.* 2010]. These criteria result in places beneath or along the margins of the late Pleistocene ice sheets being assigned to Category GIA. We assign Macdonald Observatory [Texas], which is not on the North American interior and is moving insignificantly in glacial isostatic adjustment, to Category GIA and estimate the velocity of Macdonald relative to the North American Plate interior because we wish to take advantage of the velocity tie between the SLR, GPS, and VLBI sites, all of which have a long history of observation. We omit places in Category Omit for the several reasons we state in the Notes of Table S1c.

#### 4.1.2 Places

We next assign sites to places, taking a place to consist of one to eight sites less than 30 km apart. We assume sites at a place to move at the same velocity. In this way, we evaluate the relative accuracy of the four techniques. We can more readily interpret the velocity of a place, which is the weighted mean of the velocities of nearby sites. This weighted mean also tends to average away local biases due to ground instability and water management of aquifers.

#### 4.1.3 Plate interiors and glacial isostatic adjustment

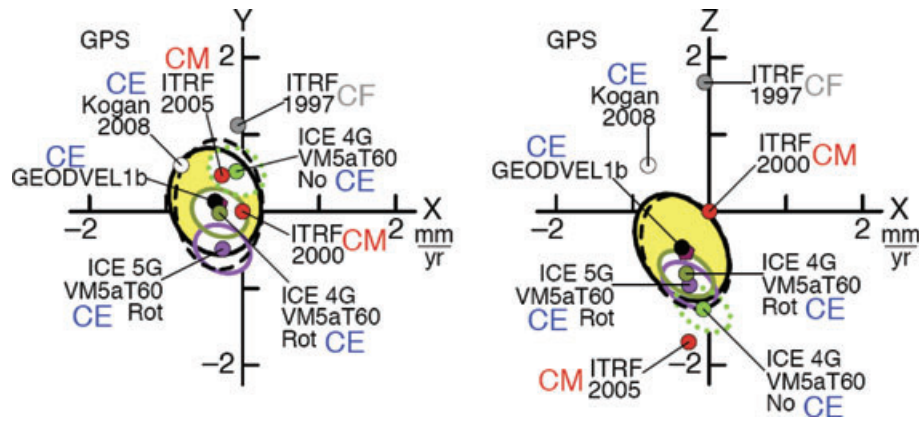
We assign places to plate interiors following the criteria of Argus & Gordon (1996), and following Argus *et al.* (1999, 2010). Places on

plate interiors are not in the belts of large and medium earthquakes, active major faults, and high topographic relief generated by active deformation. A place on a plate interior is far enough from any known fault that the interseismic strain that is accumulating causes the place to be moving relative to the plate interior more slowly than  $1 \text{ mm yr}^{-1}$ .

We next assign places to one of four categories:

Category Rigid (Table S1c) consists of places on plate interiors neither beneath nor along the margins of the former Laurentide ice sheet.

Category GIA (Table S1b) consists of places on plate interiors either beneath or along the margins of the former Laurentide ice sheets. Places in Category GIA have either uplift greater than  $2 \text{ mm yr}^{-1}$  in the model of Peltier (1996, ICE4G VM2 T120 No Rot)



**Figure 4.** Velocities between definitions of Earth's centre differently specifying the translational velocities of the GPS networks. (CM) centre of mass of Earth, oceans and atmosphere, (CE) centre of mass of solid Earth. In GEODVEL1b, we assume that, besides plate motion, the parts of the plate interiors not near the late Pleistocene ice sheets are not moving horizontally relative to CE. GEODVEL1b is nearly identical to GEODVEL (unlabeled dash black 95 per cent confidence limits) (Argus *et al.* 2009). CE Kogan 2008 is the velocity of CE that Kogan & Steblou (2008) estimate in a manner identical to that in GEODVEL1b. In ICE-5G VM5a T60 Rot, ICE-4G VM5a T60 Rot and ICE-4G VM5a T60 No Rot, we assume that the plate interiors are moving vertically and horizontally relative to CE as predicted by the postglacial rebound model. CM CSR (unlabeled maroon pentagon very near GEODVEL1b) is the velocity of CM determined by the Center for Space Research in CSR00L01, the SLR velocity model that we invert. We place the ITRF and our estimates of the velocity of Earth's centre on the same plot by estimating the translational velocity and rotational velocity between the ITRF2000 (Altamimi *et al.* 2002) site velocities and the GEODVEL1b place velocities.

or horizontal movement greater than 0.5 mm yr<sup>-1</sup> in the model of Peltier (1994, ICE-4G VM1 T120 No Rot; see Notes of Table 2b).

Category Omit (Table S1c) consists of 23 places on plate interiors that we do not use to constrain the postglacial rebound models for several reasons (see Notes of Table S1c).

Category Boundary consists of places in the deformation zones between the plate interiors. We omit places in Category Boundary.

#### 4.2 Inversion

If we were to evaluate the postglacial rebound models in straightforward fashion, we would invert the velocity estimates of sites in Category Rigid and Category GIA using the following relationship between data, parameters, and postglacial rebound predictions:

$$\mathbf{v}_{it} - \mathbf{w}_{gia} = (\boldsymbol{\omega}_a + \mathbf{R}_i) \times \mathbf{r}_i + \mathbf{T}_t, \quad (1)$$

where all quantities are 3-D vectors  $\mathbf{v}_{it}$  (a datum) is the velocity of site  $i$  estimated using space technique  $t$ ,  $\mathbf{w}_{gia}$  is postglacial rebound model prediction of the velocity of site  $i$ ,  $\boldsymbol{\omega}_a$  (a parameter) is the angular velocity of the plate the site is on,  $\mathbf{R}_i$  (a parameter) is the angular velocity of the reference frame of the space technique of the site,  $\mathbf{T}_t$  (a parameter) is the translational velocity of the reference frame of the space technique of the site (which is the negative of the velocity of CE relative to the site network of the technique), and  $\mathbf{r}_i$  (a constant) is the vector from Earth's centre to the site.

However in this study we invert the velocity estimates in a slightly more sophisticated manner using the following relationship

$$\mathbf{v}_{it} - \mathbf{w}_{gia} = (\boldsymbol{\omega}_a + \mathbf{R}_i) \times \mathbf{r}_i + \mathbf{T}_t + \mathbf{u}_b, \quad (2)$$

where the vector  $\mathbf{u}_b$  (a parameter) is the velocity of place  $b$ . We vary the parameters that we estimate in three ways (following table 2 of Argus *et al.* 1999 and table 5 of Argus *et al.* 2010).

To evaluate the postglacial rebound models, we set to zero the ( $\mathbf{u}_b$ 's) velocities of places in Category Rigid and Category GIA; the velocity of a site in Category Rigid or Category GIA constrains

the ( $\boldsymbol{\omega}_a$ ) angular velocity of the plate it is on. We estimate the ( $\mathbf{u}_b$ 's) velocities of places in Category Omit, but do not assign places in Category Omit to a plate. These inversions yield estimates of the velocity of Earth's centre (Fig. 4, PGR models) and is the basis of Figs 5–12 and S1–S5, excepting the figures stated in the next paragraph.

To determine GEODVEL1b, we set to zero the horizontal components of the ( $\mathbf{u}_b$ 's) velocities of places in Category Rigid; the velocity of a site in Category Rigid constrains the ( $\boldsymbol{\omega}_a$ ) angular velocity of the plate it is on. We estimate the ( $\mathbf{u}_b$ 's) velocities of places in Category GIA and Category Omit, but do not assign places in Category GIA or Category Omit to a plate. Assuming the velocity of 2 or more sites at a place to be equal constrains the translation velocity and rotation velocity between the reference frames of the input velocity solutions. This inversion yields an estimate of the velocity of Earth's centre (Fig. 4, GEODVEL1b) and estimates of place velocity that do not depend on a postglacial rebound model (Figs 6a, 8, 10, 11a, 13, S1 and Table S1).

We tie CBN sites to the GPS, VLBI and DORIS networks at 21 places. We tie the BIFROST velocity sites to the GPS, VLBI and DORIS networks at 16 places. In the inversion we treat correlations between all components of site velocity. But the point positioning method used for GPS and DORIS yields correlations of zero; and for VLBI and SLR the random errors embedded in the correlations tend to be less than the systematic error that we add to obtain our realistic error budget.

#### 4.3 Error budget

We formulate a realistic error budget following the method of Argus & Gordon (1996), Argus (2007) and Argus *et al.* (2010). We take the true standard error in a site velocity component to be the root sum square of a random error and a systematic error. The random error comes from the dispersion of positions about a constant velocity (for VLBI and SLR) or about a constant velocity and a sinusoid having a period of 1 yr (for GPS and DORIS). We compute the systematic error to be a distance (in mm) as we describe

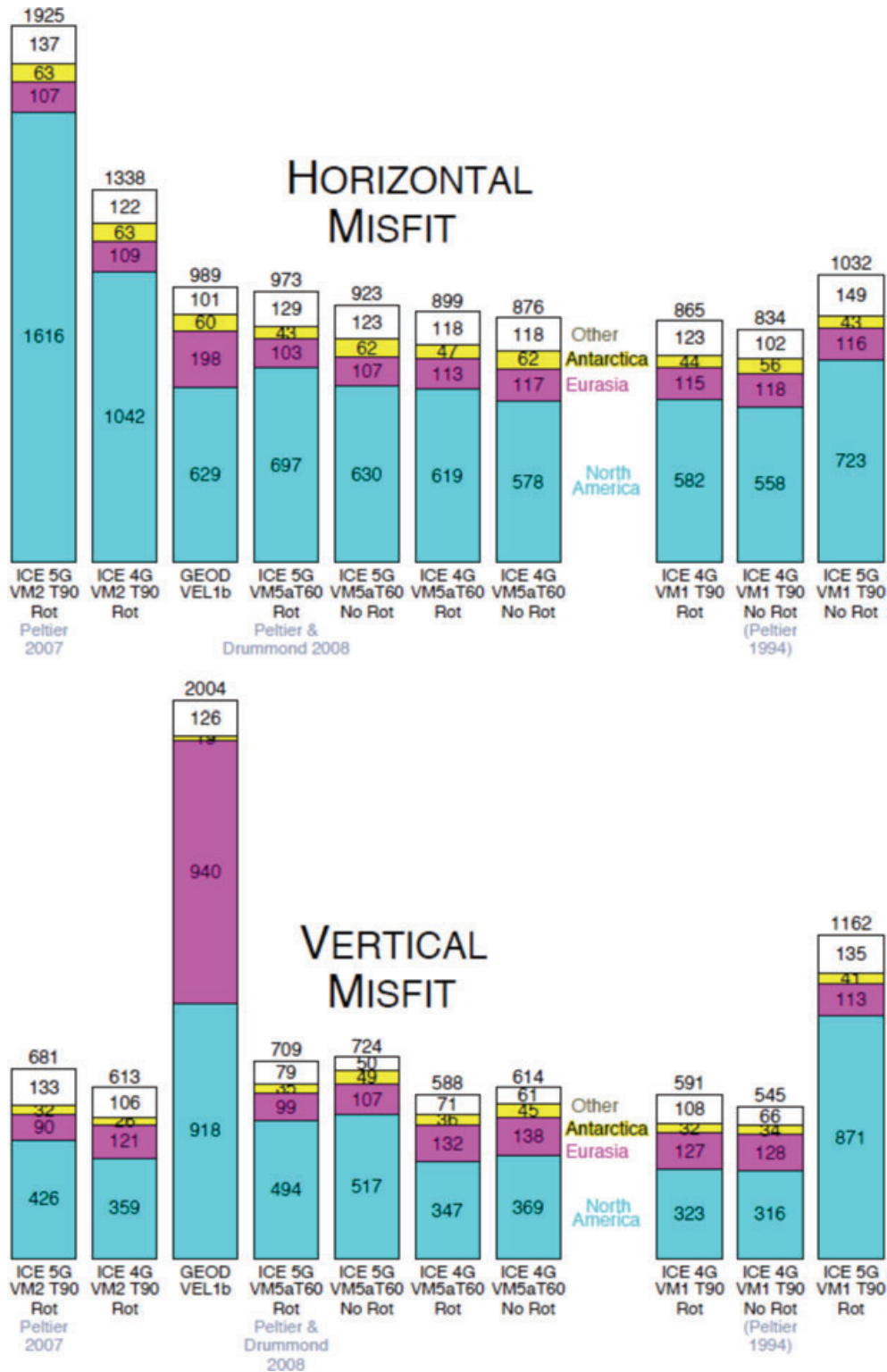


**Figure 5.** Fits of models of postglacial rebound and rotational feedback to the vertical and horizontal observations, broken down by plate. Values of chi-square are given. For each model we estimate the angular velocities of the plates and the velocity of Earth’s centre minimizing the misfit between the model and data.

next and specify in Table 1, divided by the effective time period of observation (in yr). The effective time period of observation of a site with an offset is the root sum square of the time period before and time period after the offset. For each of the four global techniques we determine the vertical distance just large enough to make

the estimates of vertical rate consistent among the four techniques; and the horizontal distance just large enough to make the estimates of horizontal velocity consistent among the four techniques and consistent with the parts of the plate interiors not near the ice sheets being rigid (as in GEODVEL1b). In sum we make the eight

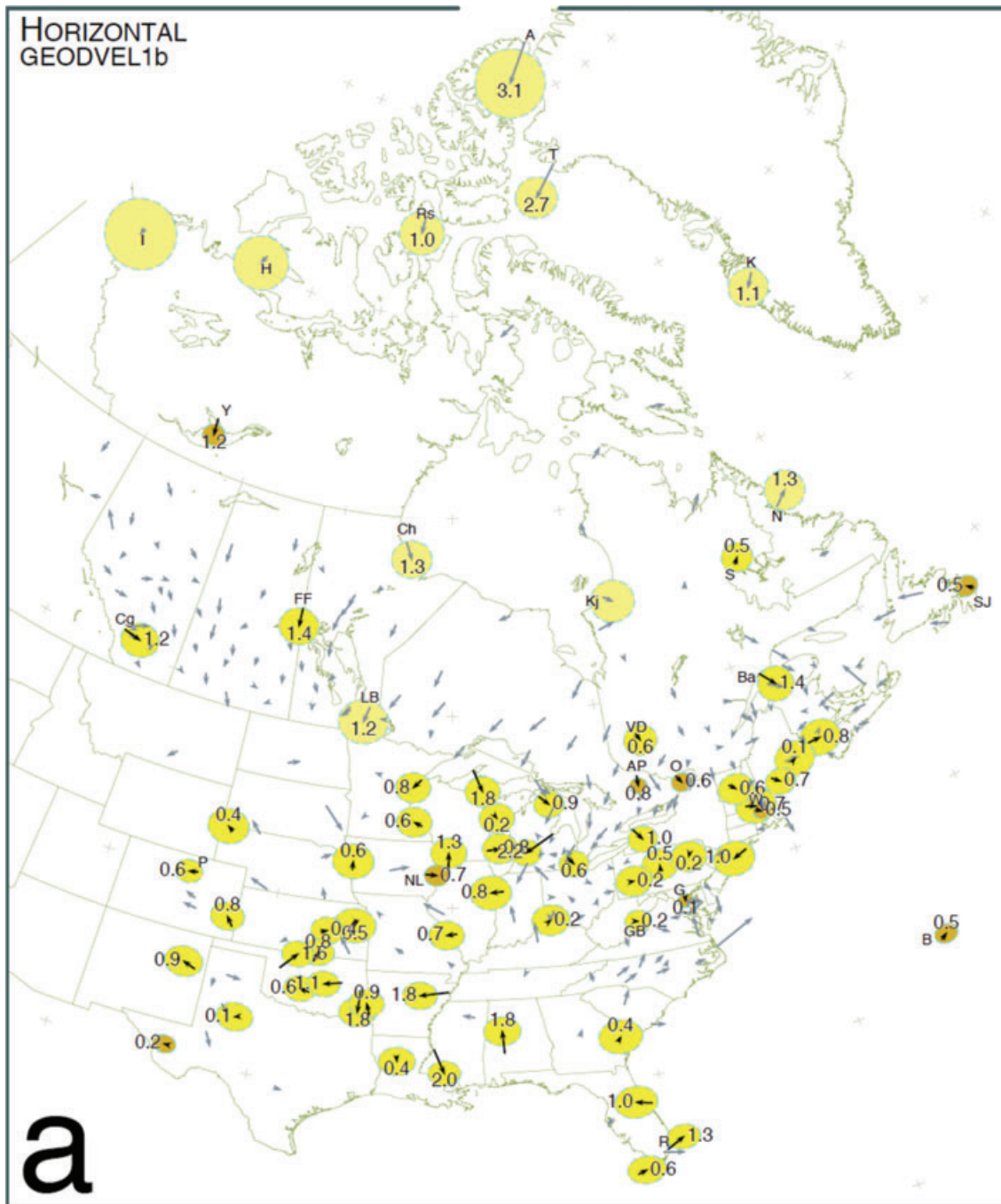


**Figure 6.** Observed horizontal velocities relative to the North American Plate in the reference frame minimizing differences with (a) a model in which [GEODVEL1b] the parts of the plate interiors not near the late Pleistocene ice sheets are not deforming laterally, (b) ICE-4G VM2 T90 Rot and (c) ICE-4G VM5a T60 Rot. In (b) and (c) red arrows show predicted velocities and are omitted where less than  $0.5 \text{ mm yr}^{-1}$ . Black arrows show well-constrained observed velocities; grey arrows show poorly constrained observed velocities. Error ellipses are 95 per cent confidence limits and are filled gold for the tightest constrained velocities (semi major axis less than  $0.5 \text{ mm yr}^{-1}$ ), filled yellow for velocities either constrained medium well (semi major axis greater than  $0.5 \text{ mm yr}^{-1}$  and less than  $0.8 \text{ mm yr}^{-1}$ ) or in the Canadian Arctic or in Greenland, and are omitted for poorly constrained velocities (semi major axis greater than  $0.8 \text{ mm yr}^{-1}$ ) elsewhere. In the horizontal illustrations (Figs 6, 11, S2 and S5) we first invert the data to estimate the best fitting parameters, next set the translational and rotational velocities of the four techniques and the angular velocities of the plates to their best fitting values and invert the data for the velocities of places on plates, then take the observed horizontal velocity to be the sum of the horizontal postglacial rebound prediction ( $w_{\text{gia}}$ ) of the place and the horizontal velocity (horizontal components of  $u_b$ ) estimated in the second inversion. See Fig. S2 for the horizontal velocities of four other postglacial rebound models.

distances just large enough to make the normalized sample standard deviations of the eight data subsets equal to one (see for example, table 4 of Argus *et al.* 1999). We assume the error budget for the campaign GPS CBN and permanent GPS BIFROST networks to be

identical to that for the global permanent GPS network. The velocity sigmas we infer are roughly comparable to those Williams *et al.* (2004) estimate using maximum likelihood estimation (see Notes of Table 1).

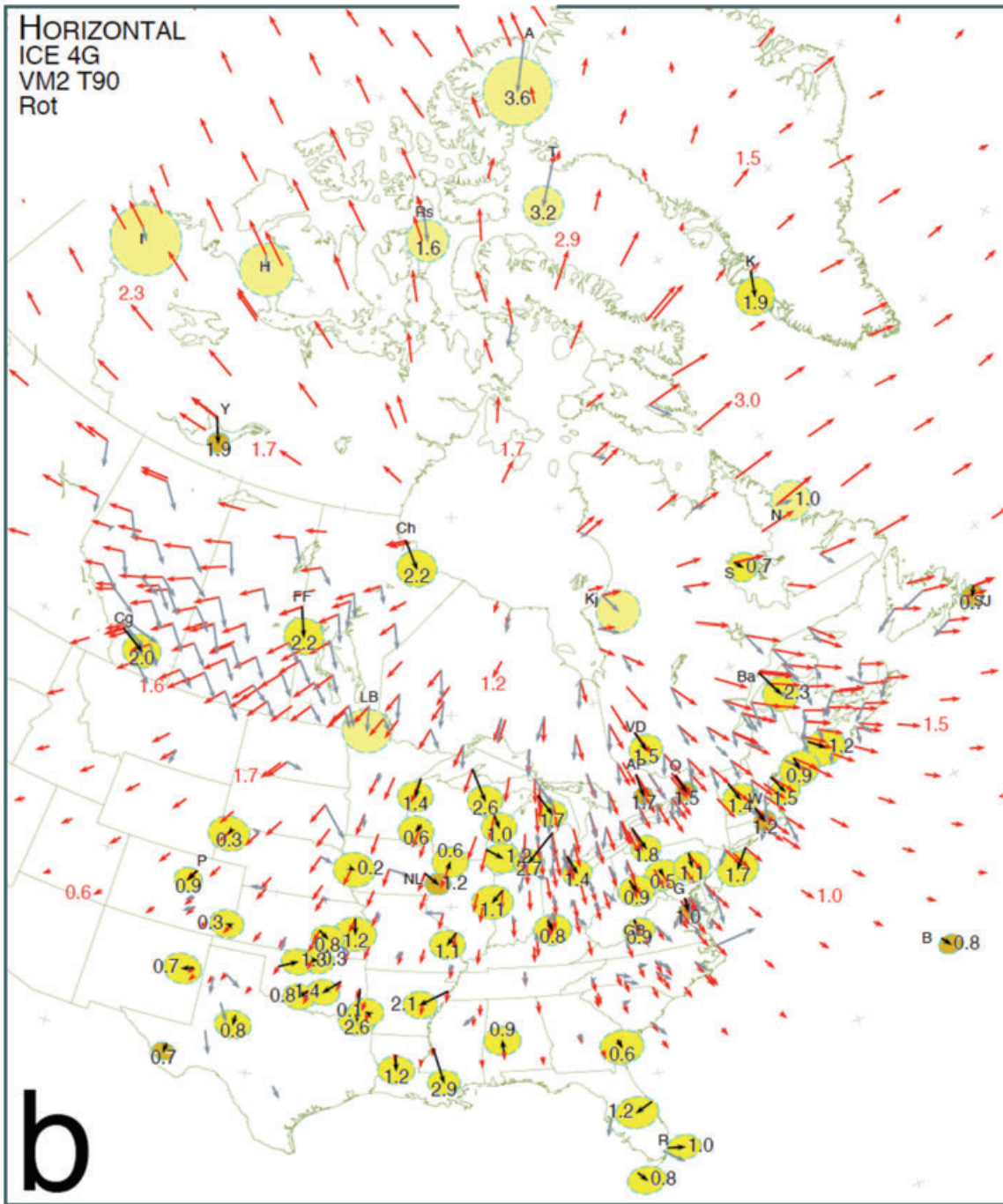


Figure 6. (Continued.)

## 5 RESULTS

### 5.1 Velocity of Earth's centre

Earth's centre is fundamental to the study of postglacial rebound because it is the point relative to which site motions are estimated (Argus 1996; Heki 1996). That is, estimates of the rate of vertical motion of a site depend entirely on the velocity of Earth's centre (Argus *et al.* 1999; Argus 2007).

The velocity of (CM) the mass centre of Earth, oceans, and atmosphere differs between ITRF2000 and ITRF2005 by  $1.8 \text{ mm yr}^{-1}$  along  $Z$  (Fig. 4). This suggests that the velocity of CM is not con-

strained very tightly by SLR observations of satellite LAGEOS (Argus 2007).

The velocity of (CE) the mass centre of solid Earth determined assuming (GEODVEL1b) that the parts of the plates not near the ice sheets are not moving relative to CE lies along  $Z \approx 1/3$  of the way from ITRF2000 to ITRF2005. The velocity of CE in GEODVEL1b is nearly identical to that in GEODVEL and to that determined using identical means by Argus (2007). But the velocity of CE along  $Z$  in GEODVEL1b differs significantly by  $\approx 1 \text{ mm yr}^{-1}$  from the velocity of CE that Kogan & Steblov (2008) estimate. Argus (2007) and Argus *et al.* (2010, Appendix A) maintain that the speed between CE and CM is less than  $0.2 \text{ mm yr}^{-1}$ .

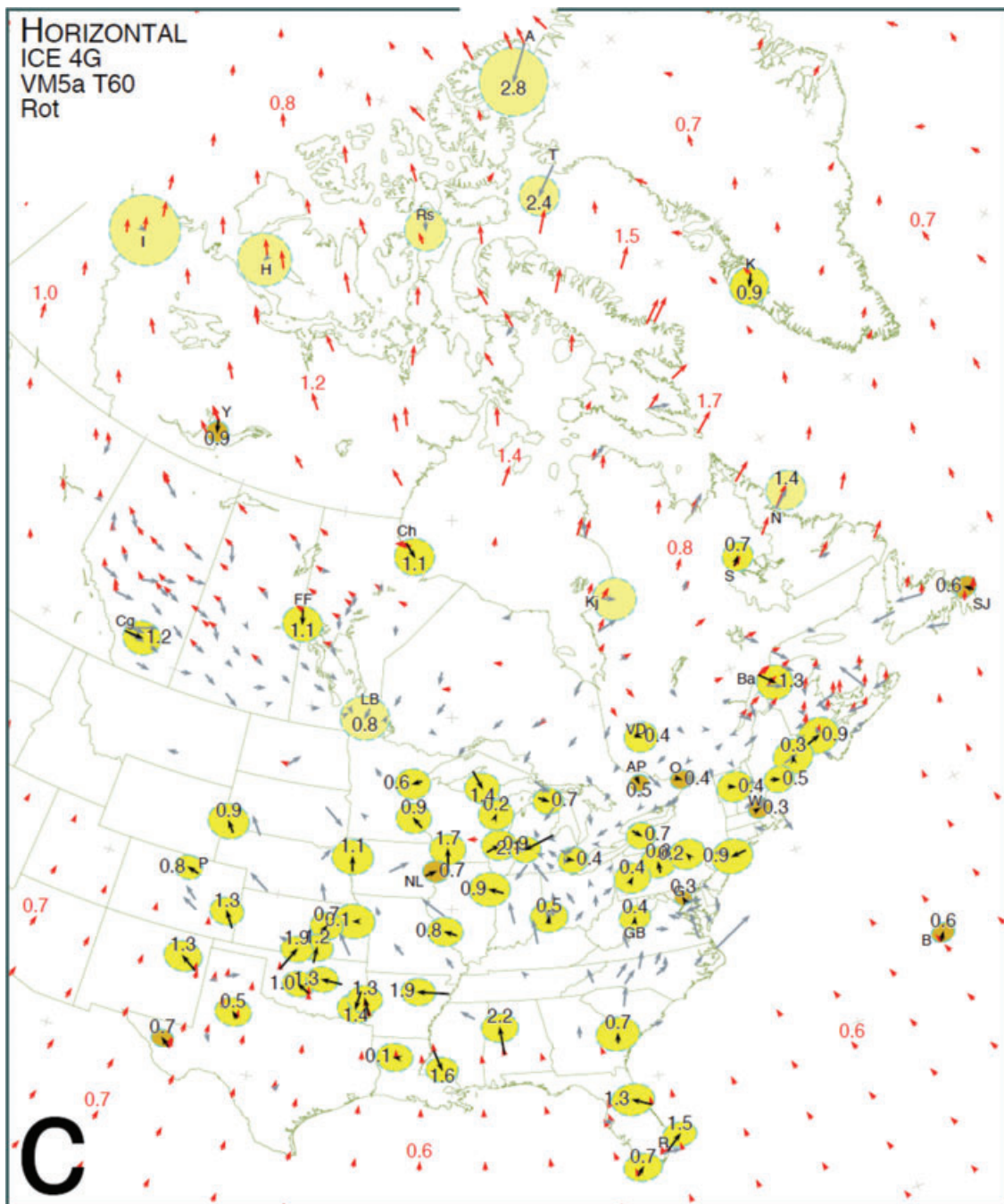


Figure 6. (Continued.)

The velocity of CE determined assuming that the plate interiors are moving as predicted by ICE-4G VM5a T60 Rot lies along Z halfway from ITRF2000 to ITRF2005. Along Y the velocity of CE in ICE-4G VM5a T60 Rot is nearer the velocity of CM in ITRF2005 than is the velocity of CE in ICE-5G VM5a T60 Rot.

In this study, we quote estimates of uplift and subsidence relative to the velocity of CE in GEODVEL1b because this definition does not depend on a specific postglacial rebound model.

## 5.2 Summary of fits of postglacial rebound models

We next describe the main results of this study (Fig. 5, Table 3). We describe misfit reductions in terms of the normalized sample

standard deviation (nssd), which is the square root of reduced chi-square). An nssd of 1.5 indicates that either the model fits the data 50 per cent worse than a perfect model, or that the data errors are 33 per cent too small. An nssd of 1 suggests that both the model fits the data well and that the data errors are realistic.

Substituting mantle and lithosphere profile VM5a T60 for VM2 T90 significantly reduces horizontal misfits in North America. The nssd decreases by a highly significant 130 per cent given ICE-5G Rot, and by a highly significant 70 per cent given ICE-4G Rot (Fig. 5, Table 3). The probability  $p$  of the misfit falling this much by chance is miniscule,  $6.1 \times 10^{-11}$  given ICE-4G Rot.

Substituting deglaciation history ICE-4G for ICE-5G reduces vertical misfits in North America by a significant ( $p = 0.00096$ )

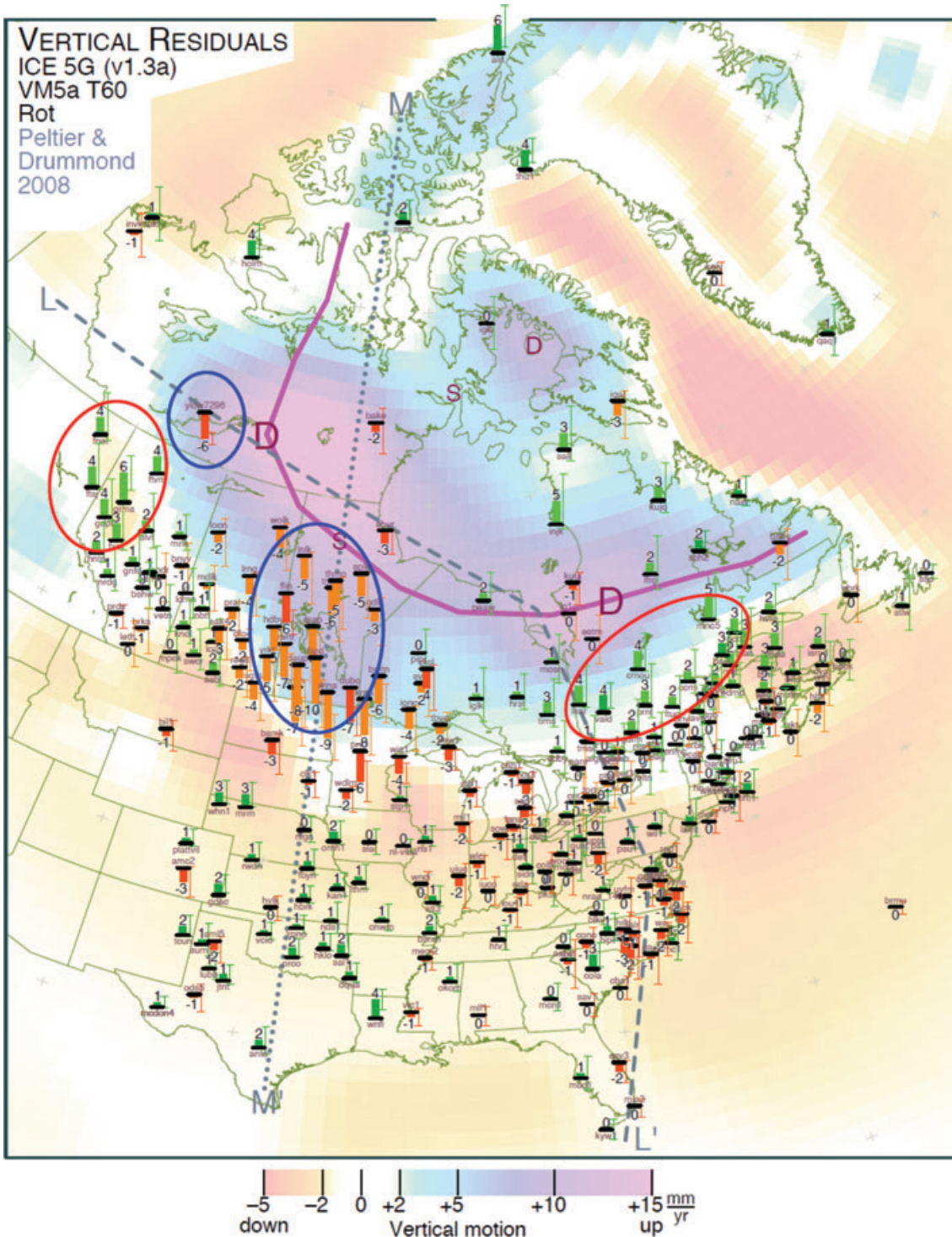


**Figure 7.** Residuals of the observed vertical rates of sites on the North American Plate interior relative to the predictions of models (a) ICE-5G VM5a T60 Rot and (b) ICE-4G VM5a T60 Rot. Green bars show positive residuals, orange bars negative residuals; Residual speeds are given in  $\text{mm yr}^{-1}$ ; Error bars are 95 per cent confidence limits; 'X's are the predictions of uplift or subsidence in the postglacial rebound model. L-L' and M-M' show the location of the profiles in Fig. 8. The colour gradations show, as the legend specifies, the predictions of the postglacial rebound model. In Fig. 7(a) the large blue and red ellipses show areas of significant misfit as stated in the text. The ice domes ('D's), ice saddles ('S's), and ice divide (thick magenta line) during last glacial maximum are from Dyke & Prest (1987, supplemental fig. 2). In the vertical illustrations (Figs 7–10, S3 and S4) we plot the vertical weighted residuals of the sites at a place. See Fig. S2 for the residuals of four other postglacial rebound models.

42 per cent (given VM5a T60 Rot). This substitution furthermore reduces horizontal misfits in North America by 26 per cent, a reduction that is insignificant ( $p = 0.070$ ), but close to the  $p = 0.05$  threshold for being 'significant'.

Substituting deglaciation history ICE-5G for ICE-4G reduces vertical misfits in Eurasia by 33 per cent (given VM5a T60 Rot). This misfit reduction is insignificant ( $p = 0.077$ ), but again marginally so.

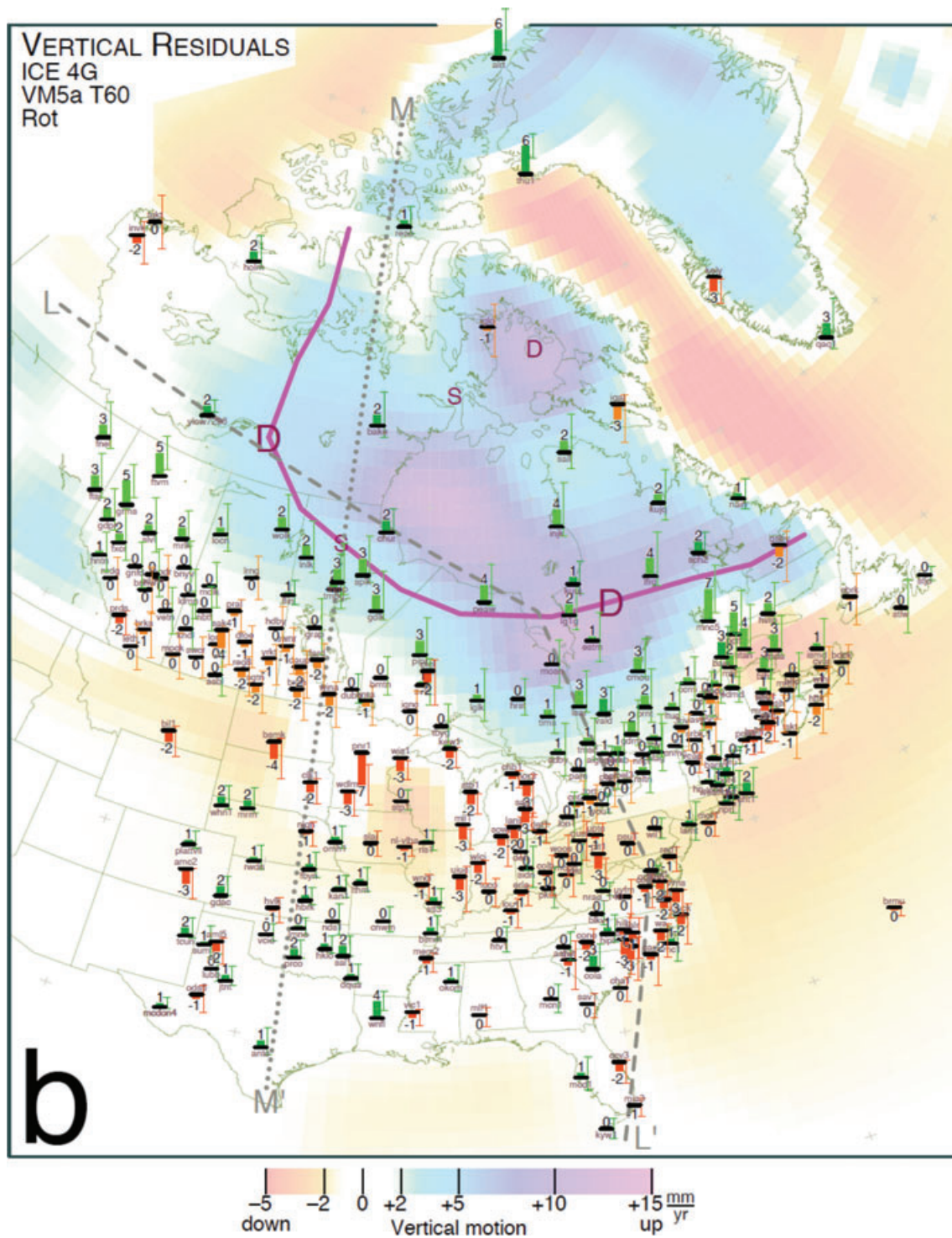
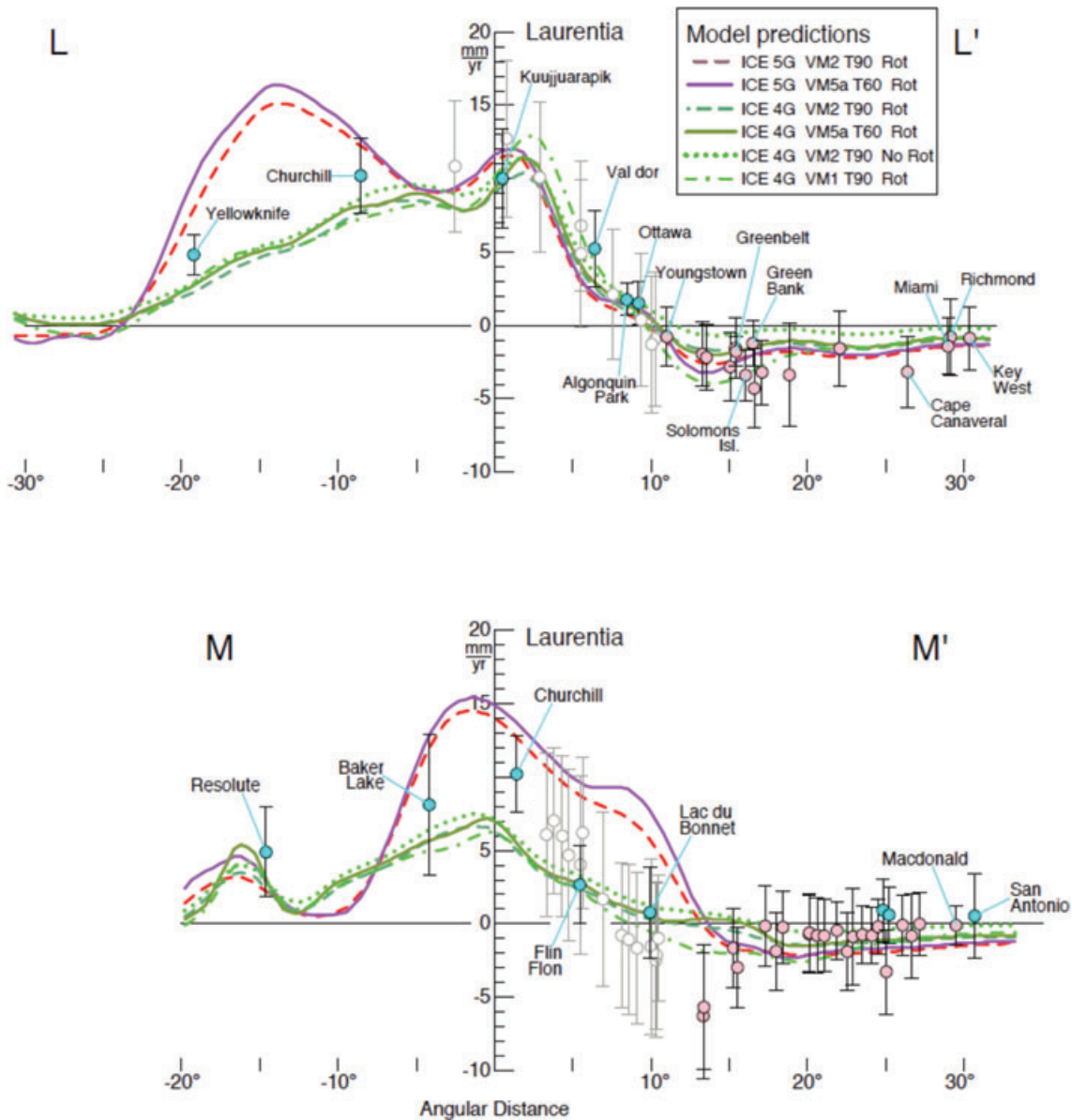


Figure 7. (Continued.)

Substituting ‘No Rot’ for ‘Rot’ changes misfits of all the data by less than 1 per cent. Substituting ‘No Rot’ for ‘Rot’ increases vertical misfits by an insignificant 4 per cent and reduces horizontal misfits by an insignificant 2 per cent (given ICE-4G VM5a T60).

Substituting mantle and lithosphere profile VM1 T90 for VM5a T60 reduces horizontal misfits by an insignificant ( $p = 0.21$ ) 6 per cent (given ICE-4G Rot). But VM1 T90 poorly fits the

McConnell spectrum describing the relaxation time of Fennoscandian rebound as a function of horizontal wave number (Peltier 2004, fig. 4). Given that pressure and temperature in the mantle increase along an adiabat except near hotspots and subduction zones, we seek a global model of postglacial rebound having a mantle viscosity fitting all RSL and space geodetic observations from the cratons. VM1 and VM2 do not; VM5a may.



**Figure 8.** Observed vertical rates of motion of places as a function of angular distance along profile L–L' and profile M–M' (Fig. 7). Blue circles show uplift and red circles subsidence of VLBI, SLR and permanent GPS sites; open circles show campaign GPS sites of the Canadian Base Network; Error bars are 95 per cent confidence limits. In the vertical profiles (Figs 8 and 10) the observed velocity is the estimated vertical component of  $\mathbf{u}_b$  in the GEODVEL1b inversion.

### 5.3 Horizontal North America

In the reference frame [GEODVEL1b] minimizing the horizontal deformation of the parts of the plate interiors not near the ice sheets, the North American Plate interior appears to be nearly rigid except for places near the margins of the former Laurentide ice sheet (Fig. 6a). The weighted root mean square residual speed of places not near the Laurentide ice sheet is  $0.9 \text{ mm yr}^{-1}$ . [The 150 FSL and CORS sites increase the dispersion from  $0.6 \text{ mm yr}^{-1}$  (in GEODVEL, Argus *et al.* 2010)]. Three places near the Laurentide ice sheet have very significant (probability less than 0.01) velocities relative to the North American Plate. Algonquin Park is moving south at  $0.8 \pm 0.5 \text{ mm yr}^{-1}$ , Yellowknife is moving south at  $1.2 \pm 0.6 \text{ mm yr}^{-1}$ , and Thule (along the east coast of Greenland) is moving southwest at  $2.7 \pm 1.2 \text{ mm yr}^{-1}$  (Table S1b). (In this study, 95 per cent confidence limits follow the ‘ $\pm$ ’.)

VM2 T90 poorly fits the horizontal observations. ICE-5G predicts the margins of the late Pleistocene Laurentide ice sheet to be moving laterally away from the ice sheet at roughly  $3 \text{ mm yr}^{-1}$  (Fig. S2a), and ICE-4G predicts the margins to be moving laterally away from the ice centre at  $\approx 2 \text{ mm yr}^{-1}$  (Fig. 6b). These predictions disagree greatly with the horizontal observations, which show the North American Plate interior to be deforming very slowly if at all. In the VM2 T90 inversions, the velocity of the North American Plate adjusts to fit the horizontal estimates of places where they are constrained tightest in eastern North America (at Greenbelt, Algonquin Park, and Westford), but that plate velocity poorly fits the horizontal estimates elsewhere [at Yellowknife, North Liberty, and Saint John’s; Figs S2a and 6b).

Substituting VM5a T60 for VM2 T90 significantly reduces horizontal misfits in North America. That is, substituting a lithosphere consisting of an upper elastic layer 60 km thick and a lower

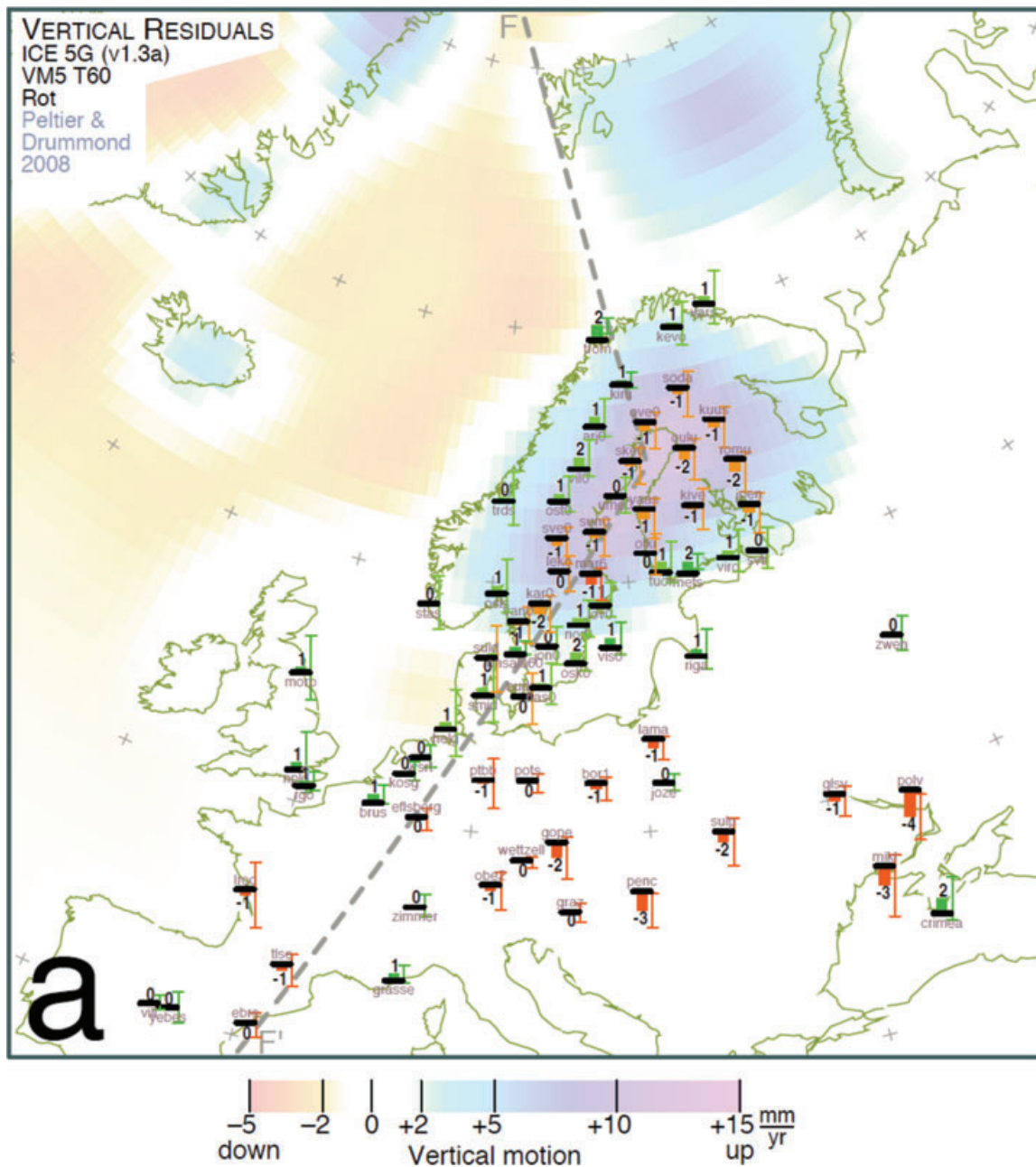


**Figure 9.** Residuals of the observed vertical rates of places on the Eurasian Plate interior relative to the predictions of model (a) ICE-5G VM5a T60 Rot and (b) ICE-5G VM5a T60. Green bars show positive residuals, orange bars negative residuals; Residual speeds are given in  $\text{mm yr}^{-1}$ ; Error bars are 95 per cent confidence limits; ‘X’s are the predictions of uplift or subsidence in the postglacial rebound model. F–F’ show the location of the profiles in Fig. 10. The colour gradations show, as the legend specifies, the predictions of the postglacial rebound model. See Fig. S3 for the residuals of four other postglacial rebound models.

high-viscosity ( $10 \times 10^{21}$  Pa s) layer 40 km thick in place of an elastic layer 90 km thick significantly reduces horizontal misfits in North America (Peltier & Drummond 2008). Given ICE-4G Rot, the nssd decreases by a highly significant 70 per cent, from 1.68 to 1.00 (Fig. 5, Table 3). The probability  $p$  of the misfit falling this much by chance is just  $6.1 \times 10^{-11}$ . VM5a T60 Rot predicts places near the margins of the ice sheet to be moving horizontally more slowly than in VM2 T90 Rot, and VM5a T60 Rot predicts the North American Plate in southern Canada and the United States to be moving horizontally hardly at all, in agreement with the observations (Figs S2b and 6c).

ICE-5G VM5a T60 Rot consists of two components, an ice sheet component (Fig. 3a) and a rotational feedback component (Fig. 3b). The ice sheet component predicts places 3000–6500 km from the centre of the former Laurentide ice sheet to be moving horizontally towards the ice sheet at  $1\text{--}1.5 \text{ mm yr}^{-1}$ . Testing this prediction is difficult because sites on the North American Plate interior are not far enough from the ice sheet centre. The rotational feedback component predicts a degree-2 order-1 pattern of horizontal velocity. In the northern United States the ice sheet and rotational feedback components are both nearly zero. In the southern United States the two components are in opposite directions and

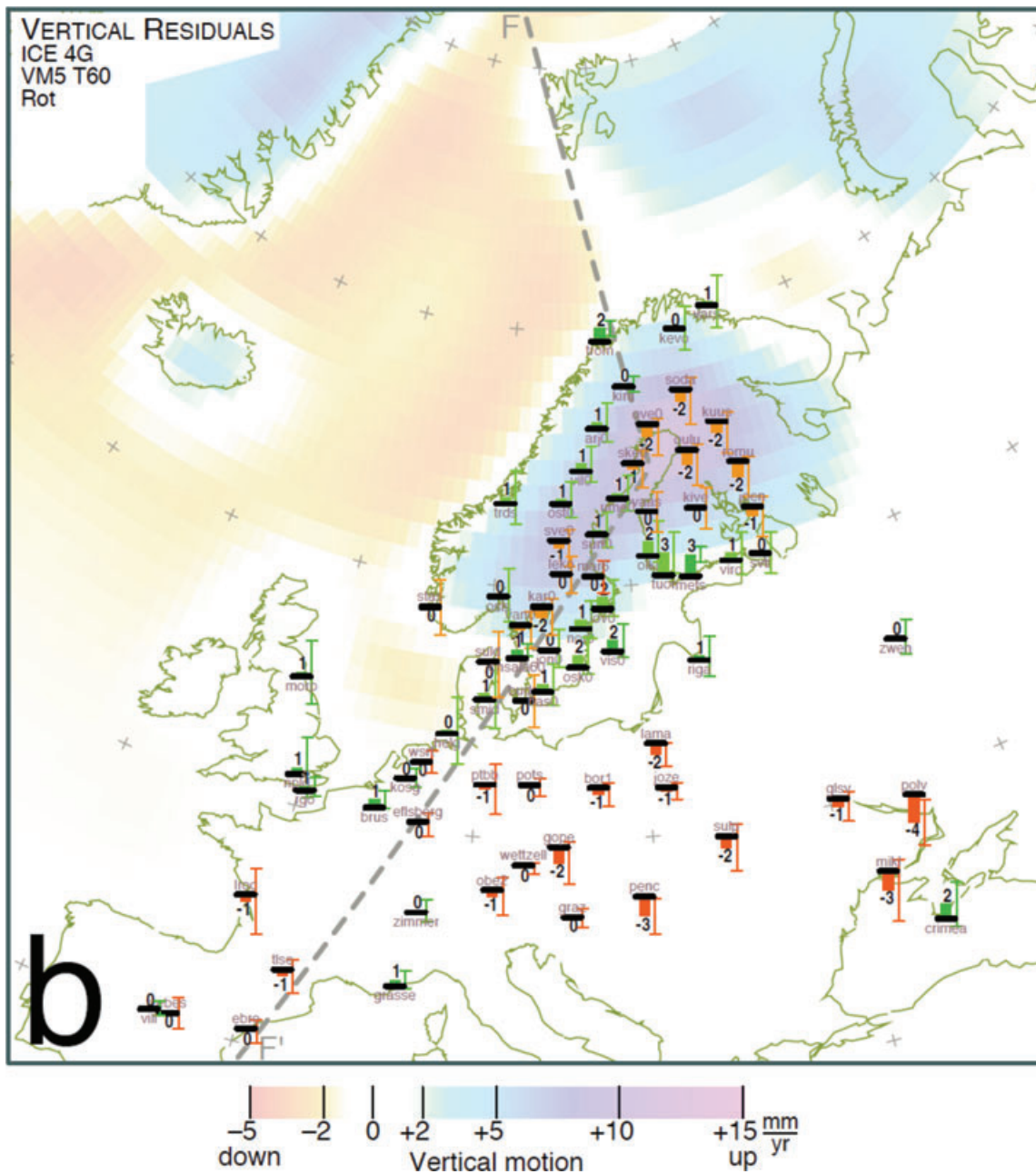


**Figure 9.** (Continued.)

cancel, summing to nearly zero. In northern Canada the two components are in the same direction and sum to  $\approx 2 \text{ mm yr}^{-1}$  towards north.

Substituting ICE-4G for ICE-5G reduces horizontal misfits in North America (given VM5a T60 Rot). The nssd decreases by 26 per cent from 1.13 to 1.00. This misfit reduction is insignificant ( $p = 0.070$ ), but close to the  $p = 0.05$  threshold for being significant. The misfit reduction is mostly due to Yellowknife [a  $\chi^2$  (chi-square) change of  $-27$ ] and Kellyville ( $-11$ ) (Figs S2b and 6c). In ICE-4G VM5a T60 Rot the ice sheet component predicts places 2000–5000 km from the centre of the former Laurentide ice sheet to be moving towards the ice sheet at  $0.6\text{--}0.8 \text{ mm yr}^{-1}$ . In ICE-4G VM5a T60 Rot the ice sheet and rotational feedback components cancel and add in the same fashion as in ICE-5G VM5a T60 Rot, but both components predict slower horizontal speeds.

The ice sheet and rotational feedback components again are nearly zero in the northern U.S., cancel to nearly zero in the southern U.S. and sum to  $\approx 1.5 \text{ mm yr}^{-1}$  towards north in northern Canada. Testing whether the far field horizontal motion towards the Laurentide ice sheet exists is difficult. ICE-4G VM5a T60 Rot predicts Richmond [Florida] to be moving north at  $0.5 \text{ mm yr}^{-1}$  and Fort Davis (Texas) to be moving north at  $0.7 \text{ mm yr}^{-1}$ . The observed horizontal velocities of the two sites are not constrained tightly enough to distinguish between these ICE-4G VM5a T60 Rot predictions and the GEODVEL1b predictions of zero.

Substituting VM1 T90 for VM5a T60 reduces horizontal misfits by an insignificant ( $p = 0.21$ ) 6 per cent. This is mostly due to Yellowknife (a  $\chi^2$  change of  $-14$ ) and Thule ( $-11$ ) (Figs S2c and 6c). But VM1 T90 poorly fits the McConnell spectrum of Fennoscandian rebound, ruling it out as a model that can fit all the observations.

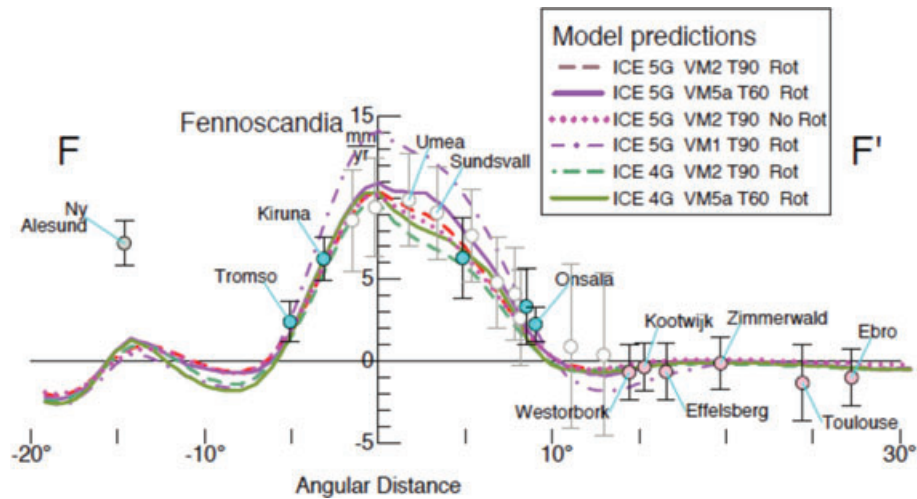


**Figure 10.** Observed vertical rates of site motion as a function of angular distance along profile F–F' (Fig. 11). Blue circles show uplift and red circles subsidence of VLBI, SLR and permanent GPS sites; open circles show permanent GPS sites of the BIFROST network; Error bars are 95 per cent confidence limits.

Next, in the vertical evaluation, we compare against VM5a T60 Rot because VM2 T90 Rot poorly fits the North America horizontal observations.

#### 5.4 Vertical North America

Substituting ICE-4G for ICE-5G reduces vertical misfits in North America by a significant ( $p = 0.00096$ ) 42 per cent (given VM5a T60 Rot). The nssd decreases from 1.58 to 1.11. This is mostly due to Yellowknife (a  $\chi^2$  change of  $-63$ , and to sites in and near southern Manitoba, including Lac du Bonnet (a  $\chi^2$  change of  $-18$ ), Flin Flon ( $-17$ ) and many CBN sites ( $-50$  for knra, fard, wina, bmtn, daup, and win5) (two areas circled by blue ellipses in Figs 7a and S3a; and Fig. 8).

Yellowknife [along the north coast of Great Slave Lake, Northwest Territories] is observed to be rising at  $4.8 \pm 1.4 \text{ mm yr}^{-1}$ ,  $6 \text{ mm yr}^{-1}$  slower than the ICE-5G prediction and  $2 \text{ mm yr}^{-1}$  faster than the ICE-4G prediction. The observation is based mainly on 12 yr of VLBI data and 10 years of GPS data (Table S1a). Therefore, near Yellowknife the Laurentide ice sheet at LGM was either thicker than in ICE-4G and much thinner than in ICE-5G or the ice came off the western part of the Laurentide ice sheet later than in ICE-4G or earlier than in ICE-5G.

Places in southern Manitoba (e.g. knra, fard, wina, win5, daup and win5) are observed to be moving vertically very slowly if at all (Fig. S1a). For example, Lac du Bonnet is observed to be rising at  $0.8 \pm 3.1 \text{ mm yr}^{-1}$ . In southern Manitoba ICE-5G predicts uplift to be  $\approx 7 \text{ mm yr}^{-1}$  faster than observed, whereas ICE-4G fits the observations well. Similarly Flin Flon (along the Manitoba–Saskatchewan border) is observed to be rising at  $2.7 \pm 2.6 \text{ mm yr}^{-1}$ ,  $6 \text{ mm yr}^{-1}$  slower than the ICE-5G prediction. If we were not to estimate 1 logged and 1 unlogged antenna offset, we would find Flin Flon to be falling at  $-0.5 \text{ mm yr}^{-1}$ .

Therefore we conclude that the 4000-km-thick ice ridge in ICE-5G at LGM extending from north to south across Lake Winnipeg did not exist; there the ice sheet at LGM was  $\approx 2000 \text{ km}$  thick as in ICE-4G. This thin ice ridge disagrees with the inference (Peltier 2004) from the terrestrial gravity data of Lambert *et al.* (2001) that there was a thick ridge in Manitoba but is consistent with the gravity

data of Pagiatakis & Salib (2003) in Saskatchewan. Given that the gravity rates of Lambert *et al.* (2001) are based on observations over just 5 yr, and given the high dispersion in their and Pagiatakis & Salib's (2003) gravity rates, we believe the terrestrial gravity data do not constrain the vertical rate of motion as strongly as do the GPS data.

Places in northern Manitoba are observed to be rising at  $\approx 6 \text{ mm yr}^{-1}$ . ICE-5G predicts uplift to be  $\approx 5 \text{ mm yr}^{-1}$  faster than observed, whereas ICE-4G predicts uplift to be  $\approx 3 \text{ mm yr}^{-1}$  slower than observed.

Churchill (along the west shore of Hudson Bay) is observed to be rising at  $10.2 \pm 2.6 \text{ mm yr}^{-1}$ ,  $3 \text{ mm yr}^{-1}$  slower than in ICE-5G and  $2 \text{ mm yr}^{-1}$  faster than in ICE-4G. Based on observations at Yellowknife, at Churchill, in northern Manitoba, at Baker Lake (northwest of Hudson Bay, Nunavut), and at Holman (Victoria Island), we deduce that the western part of the Laurentide ice sheet at LGM was intermediate in thickness between ICE-4G and ICE-5G (assuming the timing of the unloading of the ice sheet is constrained well by glacial geomorphology).

Places near the northern Alberta–British Columbia border (e.g. gdpr, ftsj and cdpr) are observed to be rising at  $\approx 5 \text{ mm yr}^{-1}$ , indicating that there the Laurentide ice sheet at LGM was thicker than in either ICE-5G or ICE-4G (area circled by red ellipse in Fig. 7a). These observations and those at Yellowknife and Holman (Victoria Island) suggest that the Keewatin ice dome at LGM was not as thick at the centre but thicker along its flanks than in ICE-5G. We are currently modifying the model of ice sheet thickness as a function of position and time to fit all the space geodetic observations.

Many places in Quebec (e.g. Schefferville, Val d'Or, mnc5, injk, lsar and cmou) have positive residuals of roughly  $3 \text{ mm yr}^{-1}$  relative to either ICE-4G or ICE-5G, suggesting that the eastern Laurentide ice sheet was slightly thicker at LGM than in either ICE-4G or ICE-5G (area circled by red ellipse in Figs 7a and S3a). Schefferville (along the Labrador–Quebec border) is rising at  $9.8 \pm 2.1 \text{ mm yr}^{-1}$ ,  $2 \text{ mm yr}^{-1}$  faster than predicted by either ICE-4G or ICE-5G. Observations along the Saint Lawrence river (e.g. baie, cnda, stan and pprt) suggest that at LGM the ice sheet extended farther south-east than in either ICE-4G or ICE-5G. Algonquin Park (Ontario) is

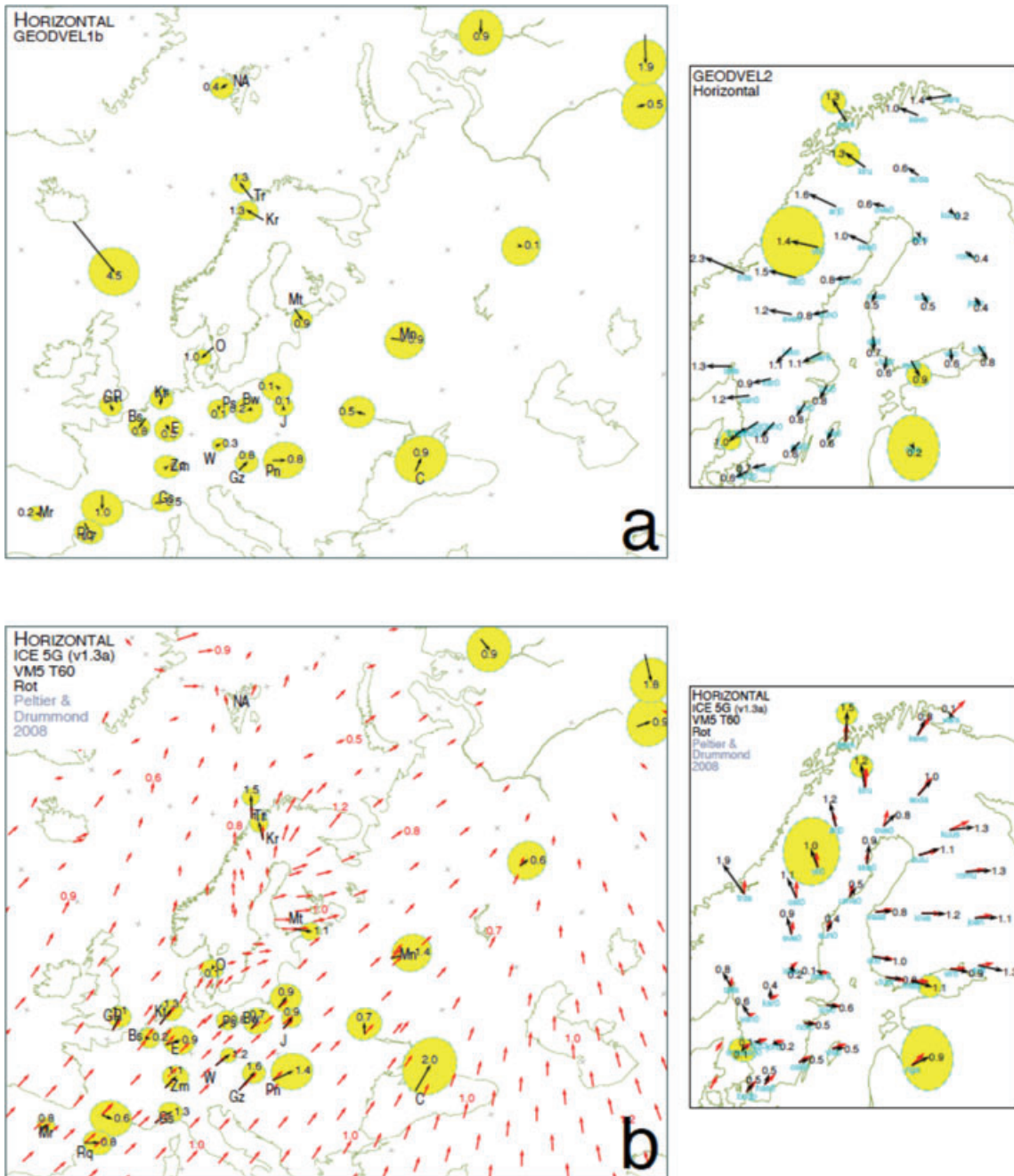


**Figure 11.** Observed horizontal velocities relative to the Eurasian Plate angular velocity in the reference frame minimizing differences with (a) the model [GEODVEL1b] in which the parts of the plate interiors not near the late Pleistocene ice sheets are rigid, (b) ICE-5G VM5a T60 Rot, (c) the ice sheet component of ICE-5G VM5a T60 Rot and (d) the rotational feedback component of ICE-5G VM5a T60 Rot. Red arrows show predicted velocities and are omitted where less than  $0.5 \text{ mm yr}^{-1}$ . Black arrows show well-constrained observed velocities; grey arrows show poorly constrained observed velocities. Error ellipses are 95 per cent confidence limits and are filled gold for the tightest constrained velocities (semi major axis less than  $0.5 \text{ mm yr}^{-1}$ ), filled yellow for velocities either constrained medium well (semi major axis greater than  $0.5 \text{ mm yr}^{-1}$  and less than  $0.8 \text{ mm yr}^{-1}$ ), and are omitted for poorly constrained velocities (semi major axis greater than  $0.8 \text{ mm yr}^{-1}$ ). The predictions in (c) and (d) total to those in (b). See Fig. S5 for model ICE-5G VM2 T90 Rot and the model's ice sheet and rotational feedback components.

observed to be rising at  $1.8 \pm 1.1 \text{ mm yr}^{-1}$ , just  $1 \text{ mm yr}^{-1}$  faster than in either ICE-4G or ICE-5G.

VM5a T60 and VM1 T90 fit all the vertical data about equally well ( $\chi^2$  difference of 2; Fig. 5, Table 3). On one hand substituting VM1 T90 for VM5a T60 reduces the vertical misfits in North America, decreasing the nssd by an insignificant 8 per cent from

1.111 to 1.032 ( $\chi^2$  change of  $-24$ ). This decrease is due to the observation that several GPS sites in the area of forebulge collapse (mil1, pit1, wis1, sag1, stb1 and pnr1) are observed to be subsiding quickly, as predicted by VM1 T90 (Figs 8 and S3c). On the other hand Westford, Greenbelt and Green Bank (VLBI and SLR sites with long histories of observation) are observed to be subsiding

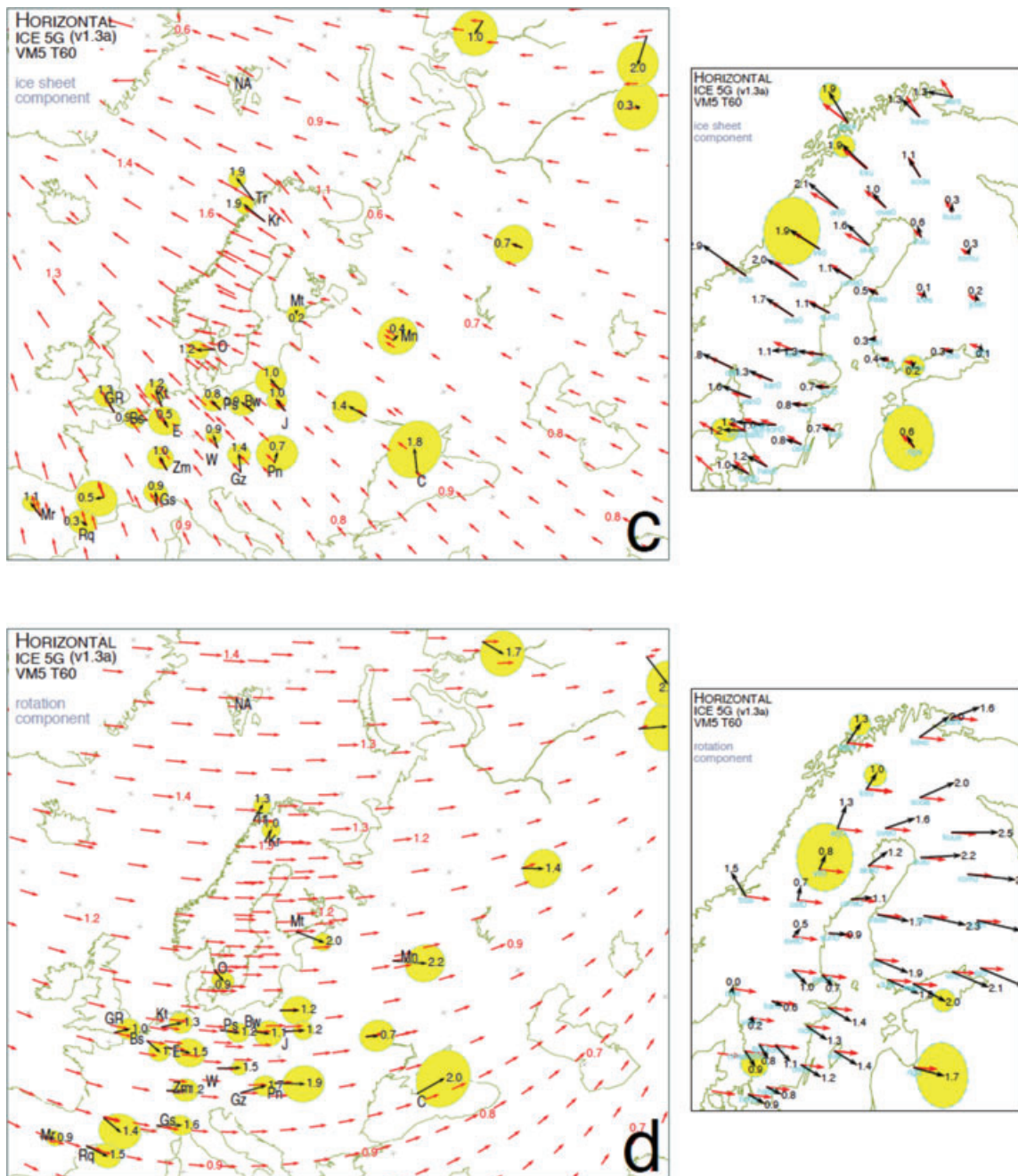


Figure 11. (Continued.)

very slowly, as predicted by VM5a T60 and Canberra and Hobart (both in Australia), on the opposite side of Earth, are moving vertically at rates agreeing better with the Earth's centre velocity in VM5a T60 than that in VM1 T90. Thus the worldwide vertical observations do not distinguish between VM1 T90 and VM5a T60. This analysis nevertheless illustrates the difficulty in distinguishing between postglacial models.

In the GEODVEL1b reference frame the weighted mean vertical rate of 163 places in the United States is subsidence at  $-1.5 \text{ mm yr}^{-1}$ . The weighted root mean square dispersion about this mean is  $1.6 \text{ mm yr}^{-1}$ . The reference frame minimizing differences with ICE-4G VM5a T60 Rot gives  $0.0\text{--}0.2 \text{ mm yr}^{-1}$  more uplift than does GEODVEL1b (Figs 7b and S1a).

### 5.5 Vertical Eurasia

Substituting ICE-5G for ICE-4G reduces vertical misfits in Eurasia by 33 per cent, decreasing the nssd from 1.32 to 1.00 (given VM5a T60 Rot). This misfit reduction is insignificant ( $p = 0.077$ ), but marginally so. The misfit reduction ( $\chi^2$  change of  $-33$ ) is mostly due to Metsahovi ( $-21$ ) and Tuoria ( $-4$ ) (Figs 9a and 9b).

ICE-5G VM5a T60 fits the vertical observations in Eurasia well. Umea, Skelleftea and Sundsvall, at the centre of Fennoscandian rebound, are estimated to be rising at  $9\text{--}10 \text{ mm yr}^{-1}$  (Fig. S1b). Tromso, Metsahovi, Kiruna and Onsala are constrained the tightest, and strongly constrain Fennoscandian rebound. Metsahovi (Finland) is estimated to be rising at  $4.0 \pm 1.3 \text{ mm yr}^{-1}$ , in agreement with ICE-5G but  $3 \text{ mm yr}^{-1}$  faster than in ICE-4G.

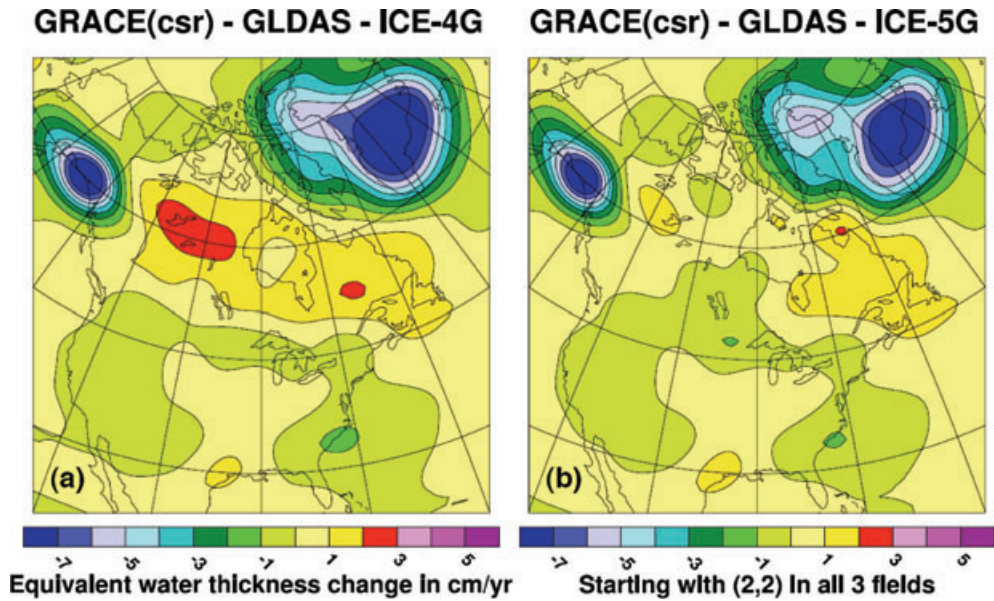


**Figure 12.** Change in equivalent water thickness estimated from GRACE observations from 2002 April to 2007 January from (CSR) Center for Space Research model RL04 less surface water change in hydrology model (GLDAS) Global Land Data Assimilation System and less the predictions of postglacial rebound models (left-hand panel) ICE-4G VM2 T90 Rot and (right-hand panel) ICE-5G VM2 T90 Rot. Stokes coefficients of degree-1, degree-2 order-0, and degree-2 order-1 are omitted in the calculation; the degree-2 order-2 coefficient and higher coefficients are included. The degree-2 order-0 coefficient is not tightly constrained by GRACE; the degree-2 order-1 coefficient records current ice mass loss in Alaska, Antarctica, Greenland, and elsewhere that is not in the postglacial rebound models. A Gaussian half width of 500 km is used. The analysis is identical to that in Peltier (2009, fig. 5).

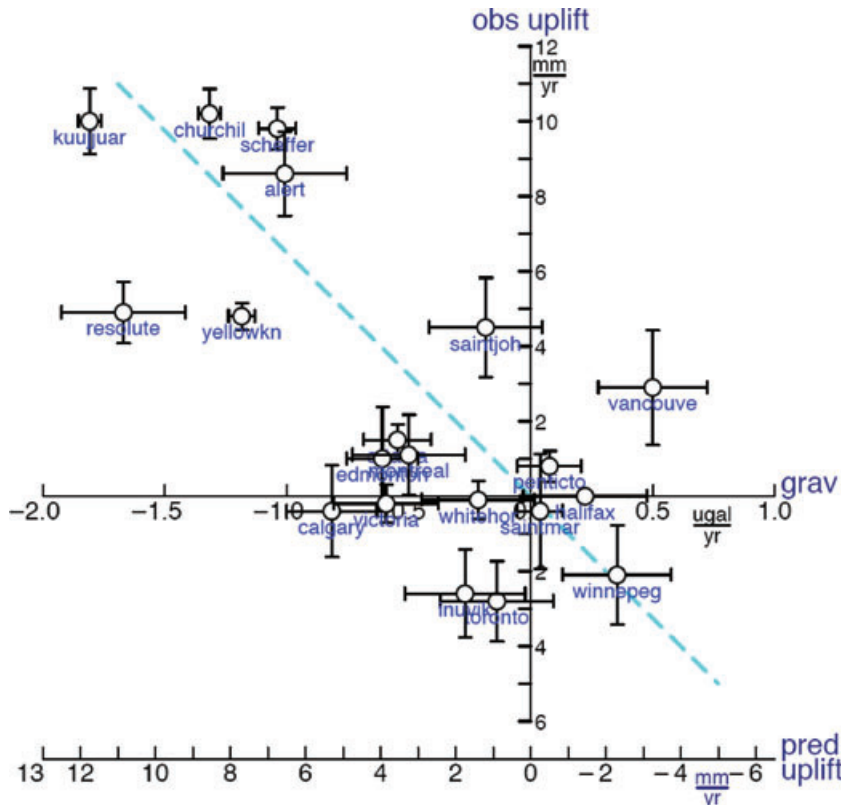


**Figure 13.** Uplift observed with GPS, VLBI, SLR and DORIS is plotted against terrestrial estimates of gravity change. Error bars are 1 sigma. GRACE and terrestrial estimates of gravity must be interpreted differently. GRACE observations of gravity are at a reference ellipsoid; terrestrial observations of gravity are at Earth's surface. Earth's surface is rising in Canada, causing a gravimeter to be moving away from Earth's centre, decreasing gravity at the site. Wahr *et al.* (1995) estimate this gravity change to be  $-1 \text{ mGal per } 6.5 \text{ mm yr}^{-1}$  uplift (bottom horizontal scale). If this ratio were exact, if the space and terrestrial observations were exact, and if Earth's water changes in Canada were negligible, then all the data would fall along the 45° dashed line. Rangelova & Sideris (2008) find that a ratio of  $-1 \text{ mGal per } 5.6 \text{ mm yr}^{-1}$  uplift minimizes differences between the terrestrial gravity and the Canada Base Network data. For more on the ratio see de Linage *et al.* (2007).

**Table 3.** Significance of differences between models.

Element 1	Element 2	Given	$\Delta\chi^2$	Nssd1	Nssd2	F	dof	$p$
North America Horizontal								
VM2 T90	VM5a T60	ICE-5G Rot	-918.9	2.609	1.126	2.317	619.7	$3.2 \times 10^{-25}$
VM2 T90	VM5a T60	ICE-4G Rot	-423.1	1.682	1.000	1.682	619.7	$6.1 \times 10^{-11}$
ICE-5G	ICE-4G	VM5a T60 Rot	-78.4	1.126	1.000	1.126	619.7	0.070
VM5a T60	VM1 T90	ICE-4G Rot	-37.3	1.000	0.939	1.065	619.7	0.21
North America Vertical								
ICE-5G	ICE-4G	VM5a T60 Rot	-146.8	1.580	1.111	1.422	313.1	0.00096
VM1 T90	VM5a T60	ICE-4G Rot	-25	1.111	1.032	1.076	313.1	0.26
Eurasia Vertical								
ICE-5G	ICE-4G	VM5a T60 Rot	-33.1	1.325	0.995	1.332	100.2	0.077
Eurasia Horizontal								
VM2 T60	VM5a T90	ICE-5G Rot	-4.2	0.555	0.534	1.040	194.2	0.39
All Vertical								
VM5a T60	VM1 T90	ICE-4G Rot	-2.5	1.291	1.286	1.004	457.8	0.48
No Rot	Rot	ICE-4G VM5a T60	-26.5	1.344	1.286	1.045	457.8	0.32
All Horizontal								
Rot	No Rot	ICE-4G VM5a T60	-22.6	1.038	1.013	1.025	882.7	0.36
Category Rigid Horizontal								
ICE-4G VM5a T60 Rot	GEODVEL1b		-13.5	1.225	1.197	1.023	483.3	0.40
ICE-4G VM5a T60 No Rot	GEODVEL1b		-36.4	1.272	1.197	1.063	483.3	0.25
Rotational feedback component of ICE-4G VM5a T60	GEODVEL1b		-71.9	1.346	1.197	1.124	483.3	0.10

Notes: Each row describes the misfit difference between two postglacial rebound models. For example (row2), substituting VM5a T60 for VM2 T90 reduces the misfit of the horizontal observations ( $\chi^2$  decrease of 423.1 given ICE-5G Rot). The normalized sample standard deviation decreases from 1.682 to 1.000. There are 619.7 degrees of freedom (dof), computing degrees of freedom using a formula ( $\text{dof} = \text{ndat} - \text{imp}$ ) in which we substitute data importance (imp) for the number of parameters in the usual formula [Bevington 1969, p. 89].  $F$  in an  $F$ -test is 1.682, indicating the misfit reduction to be statistically significant [probability ( $p$ ) =  $6.1 \times 10^{-11}$ ].

Onsala is observed to be rising at  $2.3 \pm 1.1 \text{ mm yr}^{-1}$ .

In the GEODVEL1b reference frame the weighted mean vertical rate of 42 places in continental Europe, Asia and England is subsidence at  $-0.8 \text{ mm yr}^{-1}$ . The weighted root mean square dispersion about this mean is just  $0.8 \text{ mm yr}^{-1}$ . The reference frame minimizing differences with ICE-5G VM5a T60 Rot gives  $0.3 \text{ mm yr}^{-1}$  more uplift than does GEODVEL1b (Figs 9a and S1b).

## 5.6 Horizontal Eurasia

In the reference frame (GEODVEL1b) minimizing the horizontal deformation of the parts of the plate interiors not near the ice sheets, the Eurasian Plate interior appears to be nearly rigid except for places near the former Fennoscandian ice sheet (Fig. 11a). The weighted root mean square residual speed of places not near the Fennoscandian ice sheet is  $0.6 \text{ mm yr}^{-1}$ . Places along the margins of the Fennoscandian ice sheet are moving laterally away from the ice centre. Onsala is moving south at  $1.0 \pm 0.5 \text{ mm yr}^{-1}$ , Metsahovi southeast at  $0.9 \pm 0.6 \text{ mm yr}^{-1}$ , Tromso northwest at  $1.3 \pm 0.5 \text{ mm yr}^{-1}$  and Kiruna northwest at  $1.3 \pm 0.6 \text{ mm yr}^{-1}$ .

We omit Ny Alesund and Höfn because they are moving in elastic response to current ice mass loss that is not in the postglacial rebound models. Ny Alesund, along the west coast of Spitsbergen island 110 km east of the Eurasia–North America Plate boundary, is rising at  $7.2 \pm 1.4 \text{ mm yr}^{-1}$ , in response to ice loss from glaciers to its east (Hagedoorn & Wolf 2003; Sato *et al.* 2006; Kohler *et al.* 2007) but is moving horizontally at an insignificant speed relative to the Eurasian Plate. Höfn, along the east coast of Iceland 100 km

east of the Eurasia–North America Plate boundary (Geirsson *et al.* 2006), is rising at  $13.4 \pm 3.1 \text{ mm yr}^{-1}$  and moving east relative to the Eurasian Plate at  $4.5 \pm 1.4 \text{ mm yr}^{-1}$ , in elastic response to ice loss from Vatnajökull glacier (Pagli *et al.* 2007).

Substituting VM5a T60 for VM2 T90 insignificantly ( $p = 0.39$ ) reduces horizontal misfits in Eurasia (Fig. 5, Table 3). Given ICE-5G Rot, the nssd decreases by 4 per cent, from 0.55 to 0.53. These small values of nssd suggest that the uncertainties in the horizontal velocities in Eurasia are underestimated by a factor of nearly 2.

The predictions of ICE-5G VM5a T60 Rot consist of three parts. The rotational feedback component predicts Europe to be moving east at  $\approx 1 \text{ mm yr}^{-1}$  (Fig. 11d). The Laurentide part of the ice sheet component predicts Europe to be moving northwest, at speeds increasing from  $\approx 0.8 \text{ mm yr}^{-1}$  in southeast Europe to  $\approx 1.3 \text{ mm yr}^{-1}$  in Fennoscandia (Fig. 11c). The Fennoscandian part of the ice sheet component predicts the margins of the Fennoscandian ice sheet to be moving laterally away from the ice centre at roughly  $\approx 1 \text{ mm yr}^{-1}$ .

Because the Eurasian Plate velocity in ICE-5G VM5a T60 Rot must adjust to fit the rotational feedback component and the Laurentide part of the ice sheet component, the angular velocity minimizing differences with ICE-5G VM5a T60 differs from that in GEODVEL1b. Testing whether the rotational feedback and Laurentide ice sheet components exist is difficult because the predictions change slowly across the part of the Eurasian Plate interior having sites.

ICE-5G VM5a T60 Rot predicts Tromso to be moving north at  $0.8 \text{ mm yr}^{-1}$ , more slowly than observed (Fig. 11b). And

ICE-5G VM5a T60 Rot predicts Onsala to be moving northeast at  $0.4 \text{ mm yr}^{-1}$ , more northeast than observed.

### 5.7 Rotational feedback

Rot and No Rot fit all the data about equally well (Fig. 5, Table 3). Given ICE-4G VM5a T60, substituting ‘No Rot’ for ‘Rot’ increases vertical misfits by an insignificant 4 per cent and reduces horizontal misfits by an insignificant 2 per cent. Thus the data cannot distinguish between models with and without rotational feedback, in the vertical because the velocity of Earth’s centre is uncertain, and in the horizontal because the areas of the plate interiors having geodetic sites is not large enough to detect the small differences in the predictions of rotational feedback going across the plate interiors.

### 5.8 GEODVEL1b versus ICE-4G VM5a Rot: are the parts of the plates not near the ice sheets deforming?

To further evaluate to what degree the parts of the plates not near the former ice sheets are deforming laterally, we estimate the angular velocities of the plates and the velocity of Earth’s centre best fitting the horizontal velocities of places in Category Rigid (Table 3, bottom 3 rows).

Substituting GEODVEL1b for ICE-4G VM5a T60 Rot reduces misfits by an insignificant ( $p = 0.40$ ) 2 per cent.

What if the rotational feedback component were not in the post-glacial rebound model? Substituting GEODVEL1b for ICE-4G VM5a T60 No Rot reduces misfits by an insignificant ( $p = 0.25$ ) 6 per cent. Of the total  $\chi^2$  change of  $-36$ , this is due mostly to places on the Pacific Plate ( $\chi^2$  change of  $-20$ , of which Chatham island contributes  $-13$ ), on the Antarctica Plate ( $\chi^2$  change of  $-18$ , of which Kerguelen contributes  $-13$ ), and on the Nubian Plate ( $\chi^2$  change of  $-10$ , of which Maspalomas contributes  $-8$ ). The total misfit reduction is insignificant; nevertheless these are the places at and near which more data can begin to discriminate between the two models.

What if we were to neglect the ice sheet component? Substituting GEODVEL1b for a model in which the parts of the plates not near the former ice sheets are deforming only in rotational feedback reduces misfits by an insignificant ( $p = 0.10$ ) 12 per cent. Of the total  $\chi^2$  change of  $-72$ , this is due mostly to places on the North American Plate ( $\chi^2$  change of  $-76$ ).

Thus the horizontal data cannot distinguish between a model in which the parts of the plate not near the former ice sheets are rigid and a model in which these areas are moving laterally either as predicted by rotational feedback, or towards the Laurentide ice sheet in the far field or both.

## 6 DISCUSSION

Tamisiea *et al.* (2007), Paulson *et al.* (2007) and Peltier (2009) find GRACE observations of gravity increase from 2002 to 2006 to be consistent with ICE-5G and with there being distinct ice domes east and west of Hudson Bay. In particular Peltier’s (2009) comparison suggests that the GRACE observations are more consistent with the larger size of the western Laurentide ice sheet in ICE-5G than with the smaller size in ICE-4G model (Fig. 12). Two decades ago Dyke & Prest (1987) suggested, on the basis of glacial geomorphology, that ice domes existed both west and east of Hudson Bay, as later suggested on the basis of space geodesy by Argus *et al.* (1999) & Peltier (2002b). In this study, we find that the GPS, VLBI, SLR and DORIS data suggest that the Laurentide ice sheet

at LGM was intermediate between that in ICE-5G and ICE-4G. Rangelova & Sideris (2008) also find that terrestrial gravity and the Canadian Base Network are more consistent with ICE-4G, but that the GRACE data are more consistent with ICE-5G. We expect that we can construct a model that is intermediate between ICE-4G and ICE-5G and that well fits both the GRACE observations and GPS, VLBI, SLR, and DORIS data that are analyzed herein, given that the latter data well constrain the ice sheet thickness along the southern limit of the western Laurentide ice sheet but not near its centre except at Yellowknife. The western Laurentide ice sheet must be nearly as massive as that in ICE-5G to fit the GRACE data, but the ice must be distributed more broadly across northwestern Canada in order to also fit the GPS, VLBI, SLR and DORIS observations.

Tregoning *et al.* (2009, fig. 5) find groundwater gain at Flin Flon and west of Hudson Bay to significantly affect their inference of vertical uplift from GRACE gravity observations. But we find (F.W. Landerer, personal communication, 2009) that elastic deformation generated by groundwater gain or loss from 2003 to 2008 [computed from GLDAS data using eq. (3) of Tregoning *et al.* (2009)] in most places amounts to less than  $1 \text{ mm yr}^{-1}$  of subsidence or uplift, and that groundwater gain at Flin Flon causes it to subside at just  $0.2 \text{ mm yr}^{-1}$ .

Using observations from absolute and relative gravimeters from 1961 to 1999, Pagiatakis & Salib (2003) estimate rates of surface gravity change at 64 sites in Canada. In general these terrestrial gravity observations are also consistent with an ice model that is intermediate between ICE-4G and ICE-5G and with there being distinct ice domes east and west of Hudson Bay (Pagiatakis & Salib 2003, fig. 6). However, the large dispersion in the estimated terrestrial gravity rates (Fig. 13), as evident in the many local maxima and minima on their map (Pagiatakis & Salib 2003, fig. 7), as well as the fact that the gravity rates are sensitive to fluctuations in groundwater hydrology, make them difficult to interpret. For example, the gravity data suggest Yellowknife to be rising at  $7.7 \pm 0.7 \text{ mm yr}^{-1}$ , faster than observed with mainly VLBI and GPS data and nearer the ICE-5G prediction; however these gravity data also suggest Calgary to be rising at  $5.3 \pm 2.4 \text{ mm yr}^{-1}$ , in disagreement with the observed vertical motion of nearly zero.

Using tide gauge data from 1860 to 2000, Mainville & Craymer (2005) estimate rates of lake level change at 55 sites along the shores of the Great Lakes. Although the northern shores of the Great Lakes appear to be rising and the southern shores subsiding, the tide gauge data poorly constrain the zero contour in the vertical motion of Earth’s surface because of anthropogenic management of the water levels. (For example, gates, locks, and power canals along the Saint Mary River are used to control the flow of water between Lake Superior and Lake Huron.) This is evident in the observation that contours of the rate of rise of water level do not line up between Lake Superior on the west and Lakes Huron and Michigan on the east (Mainville & Craymer 2005, fig. 5). The data constrain the gradient in the vertical motion of Earth’s surface assuming that the water level conforms to a gravitational equipotential surface. The tide gauge data suggest this gradient to be  $1.5 \text{ mm yr}^{-1}/100 \text{ km}$  going from NNE to SSW across Lake Superior, three times steeper than the gradient of  $\approx 0.6 \text{ mm yr}^{-1}$  going from NNE to SSW beginning along the northern shore of the North Channel of Lake Huron and ending at the southern tip of Lake Michigan (water levels are not being manipulated in the Straits of Mackinac between Lake Huron and Lake Michigan). It is impressive that the tide gauge data record this flattening of the vertical gradient along a traverse from the ice sheet centre that is predicted by the postglacial rebound models. ICE-4G

VM1 T90 Rot (the prediction is  $1.4 \text{ mm yr}^{-1}/100 \text{ km}$ ) fits the steep gradient across Lake Superior better than does ICE-4G VM5a T60 Rot (the prediction is  $0.6 \text{ mm yr}^{-1}/100 \text{ km}$ ); either of the two models fits the gentle gradient across Lakes Huron and Michigan (the VM1 T90 prediction is  $0.9 \text{ mm yr}^{-1}/100 \text{ km}$ ; the VM5a T60 prediction is  $0.5 \text{ mm yr}^{-1}/100 \text{ km}$ . (The predicted gradient in relative sea level is 12 per cent less than the predicted gradient in vertical motion; this does not change the conclusion we state next.) We agree with the inference of Mainville & Craymer (2005) that the tide gauge data favour ICE-4G VM1 T90 Rot over ICE-4G VM5a T60 Rot, but believe that the tide gauge data do not constrain the vertical gradient well enough to conclusively distinguish between the two models. [Mainville & Craymer (2005) compared against ICE-4G VM2 T90 not ICE-4G VM5a T60, but because VM5a is a three-layer approximation to VM2 in the mantle, the vertical gradient is similar in the two models (Fig. 8).]

Estimates of the location of the zero isoline separating uplift from subsidence, and the width of the subsiding belt around the late Pleistocene ice sheets depend strongly on the velocity of Earth's centre. In North America the zero isoline and subsiding belt also depend on the strength of rotational feedback; in Europe the two do not depend on the strength of rotational feedback (Fig. 3b).

In North America Sella *et al.* (2007), assuming Earth's centre to be the velocity of CM in ITRF2000, find the zero isoline to cut through the northern Great Lakes, towards the east near the Canada–United States border, and towards the west through Manitoba, Saskatchewan, and Alberta. We find, given the velocity of Earth's centre in ICE-4G VM5a T60 Rot, the zero isoline to be near theirs. The model suggests that all of the United States is subsiding at  $0.5\text{--}2 \text{ mm yr}^{-1}$ , mostly due to the subsidence generated by rotational feedback.

In Europe Nocquet *et al.* (2005), assuming Earth's centre to be the velocity of CM in ITRF2000, maintain that in Europe there is a belt 900 km wide that is subsiding at up to  $1.5 \text{ mm yr}^{-1}$  and that extends from the north coast of Germany to Italy. We find, given the velocity of Earth's centre in ICE-5G VM5a T60 Rot, that most of Europe is moving vertically at  $\approx 0 \text{ mm yr}^{-1}$ ; near Denmark there is a belt roughly 300 km wide subsiding at  $0.5\text{--}1.5 \text{ mm yr}^{-1}$  (Fig. 9a).

## 7 CONCLUSIONS

(1) The vertical observations in North America show that, relative to ICE-5G, the Laurentide ice sheet at LGM was (i) much thinner in southern Manitoba, (ii) thinner near Yellowknife (Northwest Territories), (iii) thicker in eastern and southern Quebec and (iv) thicker along the northern British Columbia–Alberta border, or that ice was unloaded from these areas later (thicker) or earlier (thinner) than in ICE-5G. The data indicate that the western Laurentide ice sheet was intermediate in mass between ICE-5G and ICE-4G. The vertical observations and GRACE gravity data together suggest that the western Laurentide ice sheet was nearly as massive as that in ICE-5G but distributed more broadly across northwestern Canada.

(2) Substituting VM5a T60 (Peltier & Drummond 2008) for VM2 T90, that is, introducing into the lithosphere at its base a layer with a high viscosity of  $10 \times 10^{21} \text{ Pa s}$ , greatly improves the fit of the horizontal observations in North America. ICE-4G VM5a T60 Rot predicts the North American Plate to be deforming slowly horizontally, in agreement with the data.

(3) ICE-5G VM5a T60 Rot well fits the vertical and horizontal observations in Europe.

(4) The rotational feedback component of the models predicts a degree-2 order-1 pattern, with maximum uplift, maximum sub-

sidence, and maximum horizontal movement of  $1.5 \text{ mm yr}^{-1}$  in ICE-5G and  $1 \text{ mm yr}^{-1}$  in ICE-4G (given VM5a T60 Rot). The ice sheet component of VM5a T60 Rot predicts places there to be in far field horizontal motion towards the Laurentide ice sheet (at  $1\text{--}1.5 \text{ mm yr}^{-1}$  at distances 3000 to 6500 km from the Laurentide ice sheet given ICE-5G, and at  $0.9\text{--}1.2 \text{ mm yr}^{-1}$  at distances 2000–5000 km given ICE-4G). The data cannot distinguish between models with and without rotational feedback, in the vertical because the velocity of Earth's centre is uncertain, and in the horizontal because the areas of the plate interiors having geodetic sites is not large enough to detect the slow differences in the predictions of rotational feedback going across the plate interiors.

## ACKNOWLEDGMENTS

We are grateful to Dr Michael Craymer and scientists at National Resources Canada for providing estimates of the velocities of sites in the Canadian Base Network. We are grateful to Dr Rosemarie Drummond (University of Toronto) for collating the predictions of the postglacial rebound models. We thank John Beavan, Kosuki Heki and an anonymous reviewer for their careful reviews. Part of this research was performed at Jet Propulsion Laboratory, California Institute of Technology, under contract with NASA. This research is also a contribution to the work of the Polar Climate Stability Network which is funded by the Canadian Foundation for Climate and Atmospheric Sciences and a consortium of Canadian universities. Additional support was provided by NSERC Discovery Grant A9627.

## REFERENCES

- Altamimi, Z., Sillard, P. & Boucher, C., 2002. ITRF2000: a new release of the international terrestrial reference frame for earth science applications, *J. geophys. Res.*, **107**(B10), 2214, doi:10.1029/2001JB000561.
- Altamimi, Z., Collilieux, X., Legrand, J., Garayt, B. & Boucher, C., 2007. ITRF2005: a new release of International Terrestrial Reference Frame based on time series of station positions and Earth Orientation Parameters, *J. geophys. Res.*, **112**, B004949, doi:10.1029/2007JB004949.
- Argus, D.F., 1996. Postglacial uplift and subsidence of earth's surface using VLBI geodesy: on establishing vertical reference, *Geophys. Res. Lett.*, **23**, 973–976.
- Argus, D.F., 2007. Defining the translational velocity of the reference frame of Earth, *Geophys. J. Int.*, **169**, 830–838, doi:10.1111/j.1365-246X.2007.03344.x.
- Argus, D.F. & Gordon, R.G., 1996. Tests of the rigid-plate hypothesis and bounds on intraplate deformation using geodetic data from very long baseline interferometry, *J. geophys. Res.*, **101**, 13 555–13 572.
- Argus, D.F. & Gross, R.S., 2004. An estimate of motion between the spin axis and the hotspots over the past century, *Geophys. Res. Lett.*, **31**, L06614, doi:10.1029/2004GL019657.
- Argus, D.F., Peltier, W.R. & Watkins, M.M., 1999. Glacial isostatic adjustment observed using very long baseline interferometry and satellite laser ranging, *J. geophys. Res.*, **104**, 29 077–29 083.
- Argus, D.F., Gordon, R.G., Hefflin, M.B., Eanes, R.J., Ma, C., Willis, P., Peltier, W.R. & Owen, S.E., 2010. The angular velocity of the plates and the velocity of Earth's center from space geodesy, *Geophys. J. Int.*, **180**, doi:10.1111/j.1365-246X.2010-x.
- Bevington, P., 1969. *Data Reduction and Error Analysis for the Physical Sciences*, McGraw-Hill Book Company, New York.
- Bos, M.S., Fernandes, R.M.S., Williams, S.D.P. & Bastos, L., 2008. Fast error analysis of continuous GPS observations, *J. Geodyn.*, **82**, 137–166, doi:10.1007/s00190-007-0165-x.

- de Linage, C., Hinderer, J. & Register, Y., 2007. A search for the ratio between gravity variation and vertical displacement due to a surface load, *Geophys. J. Int.*, **171**, 986–994, doi:10.1111/j.1365-246X.2007.03613x.
- Dyke, A.S. & Prest, V.K., 1987. Late Wisconsinian and Holocene History of the Laurentide ice sheet, *Geographie physique et Quaternaire* **41**, 237–263.
- Geirsson, H. *et al.*, 2006. Current plate movements across the Mid-Atlantic ridge determined from 5 years of continuous GPS measurements in Iceland, *J. geophys. Res.*, **111**, B09407, doi:10.1029/2005JB003717.
- Gross, R.S. & Vondrak, J., 1999. Astrometric and space-geodetic observations of polar wander, *Geophys. Res. Lett.*, **26**, 2085–2088.
- Hagedoorn, J.M. & Wolf, D., 2003. Pleistocene and Recent deglaciation in Svalbard: implications for tide-gauge, GPS and VLBI measurements, *J. Geodyn.*, **35**, 415–423.
- Heki, K., 1996. Horizontal and vertical crustal movements from three-dimensional very long baseline interferometry kinematic reference frame: implication for the reversal time scale revision, *J. geophys. Res.*, **101**, 3187–3198.
- James, T.S., Gowan, E.J., Wada, I. & Wang, K.L., 2009. Viscosity of the asthenosphere from glacial isostatic adjustment and subduction dynamics at the northern Cascadia subduction zone, British Columbia, Canada, *J. geophys. Res.*, **114**, B04405, doi:10.1029/2008JB006077.
- Johansson, J.M. *et al.*, 2002. Continuous GPS measurements of post-glacial adjustment in Fennoscandia: 1. Geodetic results, *J. geophys. Res.*, **107**(B8), 2157, doi:10.1029/2001JB000400.
- Kaufmann G. & Lambeck, K., 1997. Glacial isostatic adjustment and the radial viscosity profile from inverse modeling, *J. geophys. Res.*, **107**, 2280, doi:10.1029/2001JB000941.
- Kohler, J., James, T.D., Murray, T., Nuth, C., Brandt, O., Barrand, N.E., Aas, H.F. & Luckman, A., 2007. Acceleration in thinning rate on western Svalbard glaciers, *Geophys. Res. Lett.*, **34**, L18502, doi:10.1029/2007GL030681.
- Kogan, M.K. & Steblov, G.M., 2008. Current global kinematics from GPS (1995–2007) with the plate-consistent reference frame, 2008. *J. geophys. Res.*, **113**, B04416, doi:10.1029/2007JB005353.
- Lambert, A., Courtier, N., Sasagawa, G.S., Klopping, F., Winster, D., James, T.S. & Liard, J.O., 2001. New constraints on Laurentide post-glacial rebound from absolute gravity measurements, *Geophys. Res. Lett.*, **28**, 2109–2112.
- Leventer, A. *et al.*, 2006. Marine sediment record from East Antarctica margin reveals dynamics of ice-sheet recession, *GSA Today*, **16**(12), 4–10, doi:10.1130/GSAT01612A.1.
- Lidberg, M., Johansson, J.M., Scherneck, H.G. & Davis, J.L., 2007. An improved and extended GPS-derived 3D velocity field of the glacial isostatic adjustment (GIA) in Fennoscandia, *J. Geodyn.*, **81**, 213–230, doi:10.1007/s0019000601024.
- Mainville, A. & Craymer, M.R., 2005. Present-day tilting of the Great Lakes region based on water level gauges, *GSA Bull.*, **117**, 1070–1080, doi:10.1130/B25392.1.
- McCarthy, D.D. & Petit, G., 2004. IERS Technical Note Number 32, International Earth Rotation and Reference Systems Service Conventions (2003), Frankfurt.
- Milne, G.A., Davis, J.L., Mitrovica, J.X., Scherneck, H.G., Johansson, J.M., Vermeer, M. & Kouivula, H., 2001. Space-geodetic constraints on glacial isostatic adjustment in Fennoscandia, *Science*, **291**, 2381–2385.
- Mitrovica, J.X., Wahr, J., Matsuyama, I. & Paulson, A., 2005. The rotational stability of an ice-age earth, *Geophys. J. Int.*, **161**, 491–506, doi:10.1111/j.1365-246X.2005.02609.x
- Nocquet, J.M., Calais, E. & Parsons, B., 2005. Geodetic constraints on glacial isostatic adjustment in Europe, *Geophys. Res. Lett.*, **32**, L06308, doi:10.1029/2004GL022174.
- Pagiatakis, S.D. & Salib, P., 2003. Historical relative gravity observations and the time rate of change of gravity due to postglacial rebound and other tectonic movements in Canada, *J. geophys. Res.*, **108**(B9), 2406, B92406, doi:10.1029/2001JB001676.
- Pagli, C., Sigmundsson, F., Lund, B., Sturkell, E., Geirsson, H., Einarsson, P., Arnadóttir, T. & Hreinsdóttir, S., 2007. Glacio-isostatic deformation around Vatnajökull ice cap, Iceland, induced by recent climate warming: GPS observations and finite element modeling, *J. geophys. Res.*, **112**, B08405, doi:10.1029/2006JB004421.
- Paulson, A., Zhong, S. & Wahr, J., 2007. Inference of mantle viscosity from GRACE and relative sea level data, *Geophys. J. Int.*, **171**, 497–508.
- Peltier, W.R., 1986. Deglaciation-induced vertical motion of the North American continent and transient lower mantle rheology, *J. geophys. Res.*, **91**, 9099–9123.
- Peltier, W.R., 1994. Ice age paleotopography, *Science*, **265**, 195–201.
- Peltier, W.R., 1996. Mantle viscosity and ice-age ice sheet topography, *Science*, **273**, 1359–1364.
- Peltier, W.R., 2002a. Global glacial isostatic adjustment: paleogeodetic and space-geodetic tests of the ICE-4G (VM2) model, *J. Quater. Sci.*, **17**, 491–510.
- Peltier, W.R., 2002b. On the eustatic sea level history: Last Glacial Maximum to Holocene, *Quater. Sci. Rev.*, **21**, 377–396.
- Peltier, W.R., 2004. Global glacial isostasy and the surface of the ice-age earth: the ICE-5G (VM2) model and GRACE, *Ann. Rev. Earth planet. Sci.*, **32**, 111–149.
- Peltier, W.R., 2005. On the hemispheric origins of meltwater pulse 1a, *Quater. Sci. Rev.*, **24**, 1655–1671, doi:10.1016/j.quascirev.2004.06.023.
- Peltier, W.R., 2007. History of earth rotation, *Treat. Geophys.*, **9**, 243–293.
- Peltier, W.R., 2009. Closure of the budget of global sea level rise over the GRACE era: the importance and magnitudes of the required corrections for global glacial isostatic adjustment, *Quater. Sci. Rev.*, **28**, 1658–1674, doi:10.1016/j.quascirev.2009.04.004.
- Peltier, W.R. & Drummond, R., 2008. Rheological stratification of the lithosphere: a direct inference based upon the geodetically observed pattern of glacial isostatic adjustment of the North American continent, *Geophys. Res. Lett.*, **35**, L16314, doi:10.1029/2008GL034586.
- Peltier, W.R. & Fairbanks, R.G., 2006. Global glacial ice volume and Last Glacial Maximum duration from an extended Barbados sea level record, *Quater. Sci. Rev.*, **25**, 3322–3337.
- Peltier, W.R. & Luthcke, S.B., 2009. On the origins of Earth rotational anomalies: new insights on the basis of both “paleogeodetic” data and Gravity Recovery and Climate Experiment (GRACE) data, *J. geophys. Res.*, **114**, B11405, doi:10.1029/2009JB006352.
- Rangelova, E. & Sideris, M.G., 2008. Contributions of terrestrial and GRACE data to the study of the secular geoid changes in North America, *J. Geodyn.*, **46**, 131–143, doi:10.1016/j.jog.2008.03.006.
- Sato, T., Okuno, J., Hinderer, J., MacMillan, D.S., Plag, H.-P., Francis, O., Falk, R. & Fukuda, Y., 2006. A geophysical interpretation of the secular displacement and gravity rates observed at Ny-Alesund, Svalbard in the Arctic—effects of post-glacial rebound and present-day ice melting, *Geophys. J. Int.*, **165**, 729–743.
- Sella, G.F., Stein, S., Dixon, T.H., Craymer, M., James, T.S., Mazzotti, S. & Dokka, R.K., 2007. Observations of glacial isostatic adjustment in “stable” North America with GPS, *Geophys. Res. Lett.*, **34**, L02306, doi:10.1029/2006GL027081.
- Solheim, L.P. & Peltier, W.R., 1994. Avalanche effects in phase transition modulated thermal convection: a model of Earth’s mantle, *J. geophys. Res.*, **99**, 6997–7018.
- Stephenson, E.R. & Morrison, L.V., 1995. Long term fluctuations in the Earth’s rotation: 700 B.C. to A.D. 1990, *Phil. Trans. R. Soc. Lond., Ser. A*, **351**, 165–202.
- Svendsen, J.I. & 30 others, 2004. Late Quaternary ice sheet history of northern Eurasia, *Quater. Sci. Rev.*, **23**, 1229–1271, doi:10.1016/j.quascirev.2003.12.008.
- Tamisiea, M.E., Mitrovica, J.X. & Davis, J.L., 2007. GRACE gravity constrain ancient ice geometries and continental dynamics over Laurentia, *Science*, **24**, 881–883, doi:10.1126/science.1137157.
- Tregoning, P., Ramillien, G., McQueen, H. & Zwart, D., 2009. Glacial isostatic adjustment and nonstationary signals observed by GRACE, *J. geophys. Res.*, **14**, B06406, doi:10.1029/2008JB006161.
- Turcotte, D.L. & Schubert, G., 1982. *Geodynamics*, Cambridge University Press, Cambridge.
- Wahr, J., DaZhong, H. & Trupin, A., 1995. Predictions of vertical uplift caused by changing polar ice volumes on a viscoelastic earth, *Geophys. Res. Lett.*, **22**, 977–980.

Williams, S.D.P., Bock, Y., Fang, P., Jamason, P., Nikolaidis, R.M., Prawirodirdjo, L., Miller, L. & Johnson, D.J., 2004. Error analysis of continuous GPS position time series, *J. geophys. Res.*, **109**, B03412, doi:10.1029/2003JB002741.

## APPENDIX A: POLAR MOTION AND THE POLE TIDE

Earth's spin axis is moving relative to the surface geography of Earth; solid Earth is deforming elastically and viscously in response. The spin axis movement consists mostly of three parts.

- (1) A forced wobble having an amplitude of 0.1 arcsec (3 m) and a period of 1 yr,
- (2) A free Chandler wobble having an amplitude varying from 0.1 to 0.2 arcsec (3–6 m) and a period of 433 d.
- (3) The secular polar wander, a mean velocity of 0.0035 arcsec yr<sup>-1</sup> along the 79°W meridian.

Following the IERS 2003 conventions (McCarthy & Petit 2004), geodesists estimate site positions after subtracting away Earth's elastic response to the forced and free Chandler wobbles, but not Earth's response to polar wander. That is, geodesists correct for the pole tide by subtracting away the effect of all polar motions except secular polar wander at 0.0040 arcsec yr<sup>-1</sup> towards 78.1°W.

## SUPPORTING INFORMATION

Additional Supporting Information may be found in the online version of this article:

**Figure S1.** (a) Observed vertical rates of motion of places in North America in GEODVEL1b; Blue bars show uplift, red bars subsidence; Speeds are given in mm yr<sup>-1</sup>; Error bars are 95 per cent confidence limits. The colour gradations show, as the legend specifies, the predictions of postglacial rebound model ICE-5G VM2 T90 Rot. Deeper shades of blue and red are sites on the interior of the North American Plate used to constrain postglacial rebound; lighter shades of blue and red are sites omitted because either they are in the deforming zone between plate interiors or they are outliers in the vertical or horizontal. When we evaluate the postglacial rebound models we omit places west of the east edge of the Rocky Mountains because they are not on the interior of the North American Plate, and we omit places along the north shore of the Gulf

of Mexico are subsiding in response to a phenomenon other than postglacial rebound. Omitted places in southeastern Alaska rising in elastic response to current glacier unloading not in the postglacial rebound model. In the vertical observation illustrations (Figures S1a and S1b) the observed velocity is the estimated vertical component of  $\mathbf{u}_b$  in the GEODVEL1b inversion. (b) Observed vertical rates of motion of places in Eurasia in GEODVEL1b; blue bars show uplift, red bars subsidence; Speeds are given in mm yr<sup>-1</sup>; Error bars are 95 per cent confidence limits. The colour gradations show, as the legend specifies, the predictions of postglacial rebound model ICE-5G VM2 T90 Rot. Deeper shades of blue and red are sites on the interior of the Eurasian Plate used to constrain postglacial rebound; lighter shades of blue and red are sites omitted because either they are in the deforming zone between plate interiors or they are outliers in the vertical or horizontal. When we evaluate the postglacial rebound models we omit places west of the north edge of the Alps because they are not on the interior of the Eurasian Plate. Observed vertical rates are in the reference frame in which the velocity of Earth's centre is estimated assuming [Argus (2007), model HOR1] the parts of the plate interiors not near the late Pleistocene ice sheets are not moving horizontally relative to (CE) the mass centre of solid Earth.

**Figure S2.** Identical to Fig. 6 for models (a) ICE-5G VM2 T90 Rot, (b) ICE-5G VM5a T60 Rot (c) ICE-4G VM1 T90 Rot and (d) ICE-4G VM5a T60 No Rot.

**Figure S3.** Identical to Fig. 7 for models (a) ICE-5G VM2 T90 Rot, (b) ICE-4G VM2 T90 Rot (c) ICE-4G VM1 T90 Rot and (d) ICE-4G VM5a T60 No Rot.

**Figure S4.** Identical to Fig. 9 for models (a) ICE-5G VM2 T90 Rot, (b) ICE-4G VM2 T90 Rot, (c) ICE-5G VM1 T90 Rot and (d) ICE-5G VM5a T60 No Rot.

**Figure S5.** Identical to Fig. 11 for (a) ICE-5G VM2 T90 Rot, (b) the ice sheet component of ICE-5G VM2 T90 Rot and (c) the rotational feedback component of ICE-5G VM2 T90 Rot.

**Table S1(a).** Velocities of places in Category Rigid.

**Table S1(b).** Velocities of places in Category Glacial Isostatic Adjustment.

**Table S1(c).** Velocities of places in Category Omit.

Please note: Wiley-Blackwell are not responsible for the content or functionality of any supporting materials supplied by the authors. Any queries (other than missing material) should be directed to the corresponding author for the article.